

# Pion and sigma meson properties in a relativistic quark model

Amand Faessler <sup>\*</sup>, Th. Gutsche <sup>\*</sup>, M. A. Ivanov <sup>†</sup>, V. E. Lyubovitskij <sup>\*</sup>, P. Wang <sup>\*</sup>

<sup>\*</sup> *Institut für Theoretische Physik, Universität Tübingen,  
Auf der Morgenstelle 14, D-72076 Tübingen, Germany*

<sup>†</sup> *Bogoliubov Laboratory of Theoretical Physics,  
Joint Institute for Nuclear Research, 141980 Dubna, Russia*

## Abstract

A variety of strong and electroweak interaction properties of the pion and the light scalar  $\sigma$  meson are computed in a relativistic quark model, which is based on the linear realization of chiral symmetry. Under the assumption that the resulting coupling of these mesons to the constituent quarks is identical, the  $\sigma$  meson mass is determined as  $M_\sigma = 385.4$  MeV. We discuss in detail the gauging of the non-local meson-quark interaction and calculate the electromagnetic form factor of the pion and the form factors of the anomalous  $\pi^0 \rightarrow \gamma\gamma$  and  $\sigma \rightarrow \gamma\gamma$  processes. We obtain explicit expressions for the relevant form factors and evaluate the leading and next-to-leading orders for large Euclidean photon virtualities. Turning to the decay properties of the  $\sigma$  we determine the width of the electromagnetic  $\sigma \rightarrow \gamma\gamma$  transition and discuss the strong decay  $\sigma \rightarrow \pi\pi$ . In a final step we compute the nonleptonic decays  $D \rightarrow \sigma\pi$  and  $B \rightarrow \sigma\pi$  relevant for the possible observation of the  $\sigma$  meson. All our results are compared to available experimental data and to results of other theoretical studies.

*PACS:* 12.39.Ki, 13.25.Ft, 13.40.Gp, 13.40.Hq, 14.40.Lb

*Keywords:*  $\pi$  and  $\sigma$  meson;  $B$  and  $D$  meson; relativistic quark model; nonleptonic and electromagnetic decays.

## I. INTRODUCTION

During the last few years the physics of isoscalar scalar mesons and in particular of the  $\sigma$  meson has received an revival of interest due to substantial progress in experimental and theoretical activities [1] (for a status report see, for example, Ref. [2]). Originally, the light scalar meson  $\sigma$  was introduced as the chiral partner of the pion in the two-flavor linear  $\sigma$ -model [3,4]. The linear  $\sigma$ -model fulfils the chiral commutation relations, contains the partial conservation of the axial current (PCAC) and has a manifestly renormalizable Lagrangian. In approaches based on the linear realization of chiral symmetry (see, for

example, [5,6]) the  $\sigma$  meson serves to create spontaneous breaking of chiral symmetry, it generates the constituent quark mass and it is a relevant ingredient in explaining low-energy phenomenology ( $\pi\pi$  scattering,  $\Delta I = 1/2$  enhancement in  $K \rightarrow \pi\pi$ , attractive interaction between baryons in nuclear matter, etc.). On the other hand, the use of the linear or non-derivative  $\sigma$ -model Lagrangian leads to well-known difficulties. For example, current-algebra results cannot be reproduced at the tree level and can only be generated by mixing up different orders in the chiral expansion. For this reason, it was suggested [7] that the linear  $\sigma$ -model Lagrangian is modified in such a fashion that the results of current algebra are already produced at the tree level, while at the same time a clear chiral power counting is obtained. This modification is based on a unitary, chiral field-dependent transformation of the quark/nucleon field, which eliminates the non-derivative linear coupling of  $\pi$  and  $\sigma$  and replaces it by a nonlinear derivative coupling of the chiral rotation vector, identified as the new pion field. This construction also serves as a basis for the formulation of chiral perturbation theory (ChPT) [8], which is now considered as the realistic effective theory of low-energy hadron dynamics. In the context of the nonlinear realization of chiral symmetry a light  $\sigma$ -meson might be treated as a resonance in the  $\pi\pi$ -system [9,10]. Alternatively, for the linear case the  $\sigma$  can either be described as a member of a 4-quark multiplet [2] or as quark-antiquark resonance [11]. The different mechanisms for generating a light  $\sigma$  do not necessarily exclude each other, but could in turn be related in a way which is not completely understood yet.

Recently, the E791 Collaboration at Fermilab [12] and the BES Collaboration at BEPC [13] reported on evidence for a light and broad scalar resonance in nonleptonic cascade decays of heavy mesons. In the Fermilab experiment it was found that the  $\sigma$  meson is rather important in the  $D$  meson decay  $D \rightarrow 3\pi$  [12]. In a coherent amplitude analysis of the  $3\pi$  Dalitz plot the scalar resonance is determined with  $478_{-23}^{+24} \pm 17$  MeV and total width  $324_{-40}^{+42} \pm 21$  MeV. A fraction  $f = (46 \pm 11)\%$  of the decay mode  $D^+ \rightarrow \pi^+\pi^-\pi^+$  is generated by the intermediate  $\sigma$ -resonance channel. The measured branching ratio of the two-body decay  $D^+ \rightarrow \sigma\pi^+$  relative to the uncorrelated  $3\pi$  decay of the  $D$  meson is then deduced as  $\Gamma(\sigma\pi^+)/\Gamma(\pi^+\pi^-\pi^+) = 0.695 \pm 0.135 \pm 0.032$  [1,12]. The BES experiment [13] concentrated on the nonleptonic decay  $J/\Psi \rightarrow \sigma\omega \rightarrow \pi\pi\omega$ . The extracted values of the  $\sigma$  mass and width are:  $M_\sigma = 390_{-36}^{+60}$  MeV and  $\Gamma_\sigma = 282_{-50}^{+77}$  MeV.

Preliminary analyses of these two experiments were performed in Refs. [14–16]. In Ref. [14] the relevant coupling constants of the respective two-body decays  $D \rightarrow \sigma\pi$  and  $\sigma \rightarrow \pi\pi$  were extracted from the data of the E791 experiment [12]. A direct calculation of the  $D \rightarrow \sigma\pi$  amplitude was done in Ref. [15] in a constituent quark-meson model. Both analyses neglect the intrinsic momentum dependence of the  $D \rightarrow \sigma\pi$  transition form factor and, in the case of Ref. [14], the final state interaction in the three-body decay  $D \rightarrow 3\pi$ . The two approaches [14,15] arrive at a disagreement between the analysis of the nonleptonic two- and three-body decays of the  $D$  meson. The extracted [14] or calculated [15] coupling constant  $g_{D\sigma\pi}$  is approximately twice as large as the one deduced from experimental data on the two-body decay  $D \rightarrow \sigma\pi$  [1]. In Ref. [16] the effective coupling constant  $g_{J/\psi\sigma\omega}$  was estimated using the perturbative QCD technique. Also, the role of the light  $\sigma$  as a elementary particle [17] and as a correlated two-pion state [18] was examined in  $B \rightarrow \rho\pi$  decay.

In the present paper we consider the two-body nonleptonic decays involving the light  $\sigma$ -meson with  $D \rightarrow \sigma\pi$  and  $B \rightarrow \sigma\pi$ . We work in the framework of a QCD motivated,

relativistic quark model which implements a linear realization of chiral symmetry [19]- [21]. In this context the formalism also allows to describe the pion as a composite particle. To solidify and extend our considerations, we therefore also present a comprehensive analysis of the electromagnetic and anomaly form factors of  $\pi$  and  $\sigma$  associated with the transitions  $\pi \rightarrow \gamma\gamma$  and  $\sigma \rightarrow \gamma\gamma$ .

The specific scheme we work in can be viewed as an effective quantum field theory approach based on a Lagrangian of light and heavy hadrons (both mesons and baryons) interacting with their constituent quarks [19]- [21]. The coupling strength of a specific hadron to its constituent quarks is determined by the compositeness condition  $Z_H = 0$  [22,23], where  $Z_H$  is the wave function renormalization constant of the hadron. The compositeness condition enables to relate theories with quark and hadron degrees of freedom to effective Lagrangian approaches formulated in terms of hadron variables only (as, for example, Chiral Perturbation Theory [8] and its covariant extension to the baryon sector [24]).

Our strategy is as follows. We start with an effective interaction Lagrangian written down in terms of quark and hadron variables. Then, by using Feynman rules, the  $S$ -matrix elements describing hadron-hadron interactions are given by a set of quark diagrams. The compositeness condition is sufficient to avoid double counting of quark and hadron degrees of freedom. The Lagrangian contains only a few model parameters: the masses of light and heavy quarks, and scale parameters which define the size of the distribution of the constituent quarks inside the hadron. This approach has been previously used to compute exclusive semileptonic, nonleptonic, strong and electromagnetic decays of light and heavy hadrons [19]- [21] employing the same set of model parameters.

In such a way we consider the  $\sigma$ -meson as a quark-antiquark bound state of the light  $u$  and  $d$  flavors. We assume that the coupling strengths of both the pion and the sigma meson to the constituent quarks are identical in accordance with the linear realization of chiral symmetry. Based on this scheme the  $\sigma$  meson mass is determined as  $M_\sigma = 385.4$  MeV, which is in good agreement with the BES-result. Next we discuss in detail the gauging of the nonlocal meson-quark interaction and, for consistency, calculate the electromagnetic form factor of the pion. We then proceed with the anomalous  $\pi^0 \rightarrow \gamma\gamma$  and  $\sigma \rightarrow \gamma\gamma$  processes. Here we obtain explicit expressions for the relevant form factors and evaluate the leading and next-to-leading order for large Euclidean photon virtualities. As a result we also obtain the two-photon decay width of the  $\sigma$ -meson. We compute the strong decay width for the process  $\sigma \rightarrow \pi\pi$  and finally turn to the nonleptonic decays  $D \rightarrow \sigma\pi$  and  $B \rightarrow \sigma\pi$ . All our results are compared to available experimental data and to other theoretical studies.

The layout of the paper is as follows. In Sec. II we begin by introducing the relativistic quark model which implements a linear realization of chiral symmetry. Sec. III is devoted to the derivation of the electromagnetic properties of the  $\pi$  and  $\sigma$  mesons. In Sec. IV we examine the strong and nonleptonic decay characteristics of the transitions  $\sigma \rightarrow \pi\pi$  and  $D(B) \rightarrow \sigma\pi$ . Then in Sec. V we turn to a numerical analysis of the processes considered and discuss the quality of results in comparison with experiment and previous model calculations. Finally, we summarize our results in Sec. VI.

## II. THE MODEL

We will consistently employ the relativistic constituent quark model [19]- [21] to compute a variety of observables related to the  $\pi$  and  $\sigma$  mesons. In the following we will present details of the model which is essentially based on an effective interaction Lagrangian describing the coupling between hadrons and their constituent quarks.

The coupling of a meson  $H(q_1\bar{q}_2)$  to its constituent quarks  $q_1$  and  $\bar{q}_2$  is set up by the Lagrangian

$$\mathcal{L}_{\text{int}}^{\text{Str}}(x) = g_H H(x) \int dx_1 \int dx_2 F_H(x, x_1, x_2) \bar{q}(x_2) \Gamma_H \lambda_H q(x_1) + \text{h.c.} \quad (1)$$

Here,  $\lambda_H$  and  $\Gamma_H$  are Gell-Mann and Dirac matrices which inclose the flavor and spin quantum numbers of the meson field  $H(x)$ . The function  $F_H$  is related to the scalar part of the Bethe-Salpeter amplitude and characterizes the finite size of the meson. To satisfy translational invariance the function  $F_H$  has to fulfil the identity  $F_H(x + a, x_1 + a, x_2 + a) = F_H(x, x_1, x_2)$  for any 4-vector  $a$ . In the following we use a particular form for the vertex function

$$F_H(x, x_1, x_2) = \delta(x - w_{21}x_1 - w_{12}x_2) \Phi_H((x_1 - x_2)^2) \quad (2)$$

where  $\Phi_H$  is the correlation function of two constituent quarks with masses  $m_1, m_2$  and  $w_{ij} = m_j/(m_i + m_j)$ .

The coupling constant  $g_H$  in Eq. (1) is determined by the so-called *compositeness condition* originally proposed in [22], and extensively used in [19]- [21], [23]. The compositeness condition requires that the renormalization constant of the elementary meson field  $H(x)$  is set to zero

$$Z_H = 1 - \frac{3g_H^2}{4\pi^2} \tilde{\Pi}'_H(M_H^2) = 0 \quad (3)$$

where  $\tilde{\Pi}'_H$  is the derivative of the meson mass operator described by the Feynman diagram of Fig. 1. In the case of pseudoscalar ( $\Gamma_H = i\gamma^5$ ) and scalar ( $\Gamma_H = I$ ) mesons, relevant for the present paper, we obtain the expression

$$\tilde{\Pi}'_H(p^2) = -\frac{p^\alpha}{2p^2} \frac{d}{dp^\alpha} \int \frac{d^4k}{4\pi^2 i} \tilde{\Phi}_H^2(-k^2) \text{tr} \left[ \Gamma_H S_1(\not{k} + w_{21} \not{p}) \Gamma_H S_2(\not{k} - w_{12} \not{p}) \right], \quad (4)$$

where  $\tilde{\Phi}_H(-k^2)$  is the Fourier-transform of the correlation function  $\Phi_H((x_1 - x_2)^2)$  and  $S_i(\not{k})$  is the quark propagator. We use free fermion propagators for the valence quarks

$$S_i(\not{k}) = \frac{1}{m_i - \not{k}} \quad (5)$$

with an effective constituent quark mass  $m_i$ . As discussed in [19]- [21] we assume for the meson mass  $M_H$  that

$$M_H < m_1 + m_2 \quad (6)$$

in order to avoid the appearance of imaginary parts in the physical amplitudes. The calculational technique for determining the explicit expression of  $\tilde{\Pi}'_H(p^2)$  (4) is outlined in Appendix A.

In accordance with the two-flavor linear  $\sigma$ -model [3,4] the universal interaction of  $\pi$  and  $\sigma$  to constituent quarks is

$$\mathcal{L}_{\text{int}}^{\text{Str};\pi+\sigma}(x) = \frac{g}{\sqrt{2}} \int dy \Phi(y^2) \bar{q}(x+y/2) [\sigma(x) + i\gamma^5 \vec{\pi}(x) \vec{\tau}] q(x-y/2). \quad (7)$$

where the identities  $g \doteq g_\pi \equiv g_\sigma$  and  $\Phi \doteq \Phi_\pi \equiv \Phi_\sigma$  are required by chiral symmetry. With the constraints set by the linear  $\sigma$ -model, the compositeness condition of Eq.(3) allows to determine the  $\sigma$  meson mass by the equality

$$\tilde{\Pi}'_\sigma(M_\sigma^2) = \tilde{\Pi}'_\pi(M_\pi^2), \quad (8)$$

where the physical pion mass  $M_\pi$  is used as an input.

The  $S$ -matrix elements describing hadronic transitions are given by a set of quark diagrams. The corresponding  $S$ -matrix operator is constructed with the use of the interaction Lagrangian

$$\mathcal{L}_{\text{int}} = \mathcal{L}_{\text{int}}^{\text{Str}} + \mathcal{L}_{\text{int}}^{\text{EW}}. \quad (9)$$

It includes the strong interaction part  $\mathcal{L}_{\text{int}}^{\text{Str}}$ , as already defined by Eqs. (1) or (7), modeling the transition of the hadron to the constituent quarks. The electroweak part  $\mathcal{L}_{\text{int}}^{\text{EW}}$  contains the coupling of hadrons and quarks with the electromagnetic and weak gauge bosons as taken from the Standard Model. For the specific processes considered, we need the interaction Lagrangian of charged pions and quarks with the electromagnetic field and the one responsible for the nonleptonic  $cd \rightarrow ud$  and  $bu \rightarrow ud$  transitions [25].

The electromagnetic interaction Lagrangian contains two parts. The first term is generated, as usual, from the free Lagrangian by minimal substitution:

$$\mathcal{L}_{\text{int};1}^{em}(x) = -eA_\mu(x) [\bar{q}(x) \gamma^\mu Q q(x) + \pi^-(x) i \overleftrightarrow{\partial}^\mu \pi^+(x)] + e^2 A_\mu^2(x) \pi^+(x) \pi^-(x) \quad (10)$$

where  $A \overleftrightarrow{\partial}^\mu B \equiv A \partial^\mu B - B \partial^\mu A$ . To guarantee local gauge invariance of the strong interaction Lagrangian, in  $\mathcal{L}_{\text{int}}^{\text{Str}}$  we multiply each quark field  $q(x_i)$  with the gauge field exponential

$$q(x_i) \rightarrow \exp \left\{ i e Q \int_x^{x_i} dz_\mu A^\mu(z) \right\} q(x_i) \quad (11)$$

where  $Q$  is the quark charge matrix. Then the second term of the electromagnetic interaction Lagrangian  $\mathcal{L}_{\text{int};2}^{em}$  arises, when expanding the gauging exponential up to a certain power of  $A_\mu$ , relevant for the order of perturbation theory and for the process we consider. For example, for the electromagnetic transition  $\sigma \rightarrow \gamma\gamma$  the responsible interaction term is given by:

$$\mathcal{L}_{\text{int};2}^{em}(x) = \frac{g}{\sqrt{2}} \sigma(x) \int dx_1 \int dx_2 F_H(x, x_1, x_2) \bar{q}(x_2) \left[ I_Q(x_1, x_2, P) + \frac{1}{2} I_Q^2(x_1, x_2, P) \right] q(x_1) \quad (12)$$

where

$$I_Q(x, y, P) = i e Q I(x, y, P), \quad I(x, y, P) = \int_y^x dz_\mu A^\mu(z)$$

and  $P$  designates the path from  $y$  to  $x$ . We use a formalism [19,26,27] which is based on the path-independent definition of the derivative of  $I(x, y, P)$ :

$$\lim_{dx^\mu \rightarrow 0} dx^\mu \frac{\partial}{\partial x^\mu} I(x, y, P) = \lim_{dx^\mu \rightarrow 0} [I(x + dx, y, P') - I(x, y, P)] \quad (13)$$

where path  $P'$  is obtained from  $P$  when shifting the end-point  $x$  by  $dx$ . Use of the definition (13) leads to the key rule

$$\frac{\partial}{\partial x^\mu} I(x, y, P) = A_\mu(x) \quad (14)$$

which in turn states that the derivative of the path integral  $I(x, y, P)$  does not depend on the path  $P$  originally used in the definition. The non-minimal substitution (11) is therefore completely equivalent to the minimal prescription as evident from the identities (13) or (14). The method of deriving Feynman rules for a non-local coupling of hadrons to photons and quarks was already developed in Refs. [19,27] and will be discussed in the next section, where we apply the formalism to the physical processes considered here.

The effective interaction Lagrangian relevant for the nonleptonic two-body decays  $D \rightarrow \sigma\pi$  and  $B \rightarrow \sigma\pi$  is given by [25]:

$$\mathcal{L}_{\text{int}}^{nl} = -\frac{G_F}{\sqrt{2}} \left\{ V_{cd}^* V_{ud} [c_1^{(c)} O_1^{(c)} + c_2^{(c)} O_2^{(c)}] + V_{ub}^* V_{ud} [c_1^{(b)} O_1^{(b)} + c_2^{(b)} O_2^{(b)}] \right\} + \text{H.c.} \quad (15)$$

where  $G_F$  is the Fermi coupling constant and  $V_{qq'}$  are the matrix elements of the Cabibbo-Kabayashi-Maskawa quark-mixing matrix ( $V_{cd}^* V_{ud} = 0.217$  and  $V_{ub}^* V_{ud} = 0.0036$ ) [1]. The four-quark operators  $O_i^{(Q)}$ , weighted by the Wilson coefficients  $c_i^{(Q)}$ , are defined as:

$$\begin{aligned} O_1^{(c)} &= (\bar{d}_i c_i)_{V-A} (\bar{u}_j d_j)_{V-A}, & O_2^{(c)} &= (\bar{d}_i c_j)_{V-A} (\bar{u}_j d_i)_{V-A}, \\ O_1^{(b)} &= (\bar{u}_i b_i)_{V-A} (\bar{d}_j u_j)_{V-A}, & O_2^{(b)} &= (\bar{u}_i b_j)_{V-A} (\bar{d}_j u_i)_{V-A} \end{aligned} \quad (16)$$

where  $i, j$  are the color indices and label  $V - A$  is a short-hand notation for the  $\gamma^\mu(1 - \gamma^5)$  Dirac structure. Under the naive factorization hypothesis [28], the particular combination of Wilson coefficients  $a_1^{\text{F};(Q)} = c_1^{(Q)} + c_2^{(Q)}/N_c$  contributes to the decay amplitudes  $D \rightarrow \sigma\pi$  and  $B \rightarrow \sigma\pi$ , where  $N_c = 3$  is the number of colors. When taking into account additional nonfactorizable contributions we have [29]:

$$a_1^{\text{F+NF};(Q)} = c_1^{(Q)} + c_2^{(Q)} \left( \frac{1}{N_c} + \chi_1^{(Q)} \right) \quad (17)$$

where the parameter  $\chi_1^{(Q)}$  encompasses the nonfactorizable effects including vertex corrections, hard spectator interactions, final-state interaction effects, resonance effects, etc. The nonfactorizable term  $\chi_1^{(Q)}$  compensates the scale and scheme dependence of the Wilson coefficients to finally render  $a_1^{(Q)}$  physical. For charm decays it was found [29], that an occurring

discrepancy between theory and experiment is greatly diminished if the Fierz transformed term in  $a_1^{F;(c)}$  is dropped, which corresponds to the large  $N_c$ -limit. Based on this observation  $\chi_1^{(c)}$  should be chosen as  $\chi_1^{(c)} = -1/N_c$ . For bottom decays  $\chi_1^{(b)}$  was found to be positive [30]. Finally, we use the following values for the effective couplings  $a_1^{F+NF;(Q)}$  in the nonleptonic transition processes:  $a_1^{F+NF;c} = 1.274$  [29] and  $a_1^{F+NF;b} = 1.038$  [30].

Transition matrix elements involving composite hadrons are specified in the model by the appropriate quark diagram. For example, the transition form factor which characterizes the hadronic transition  $H_{13}(p_1) \rightarrow H_{23}(p_2) + H_{12}(p_3)$  is determined from the Feynman integral corresponding to the diagram of Fig. 2:

$$\begin{aligned} \Lambda^{12;13;23}(p_1, p_2) &= \frac{3}{4\pi^2} g_{H_{13}} g_{H_{23}} g_{H_{12}} I^{12;13;23}(p_1, p_2) \\ I^{12;13;23}(p_1, p_2) &= - \int \frac{d^4 k}{4\pi^2 i} \tilde{\Phi}_{H_{13}}(-(k + w_{13} p_1)^2) \tilde{\Phi}_{H_{23}}(-(k + w_{23} p_2)^2) \\ &\quad \times \tilde{\Phi}_{H_{12}}(-(k + w_{12} p_1 + w_{21} p_2)^2) \text{tr}[S_2(\not{k} + \not{p}_2) \Gamma_{H_{12}} S_1(\not{k} + \not{p}_1) \Gamma_{H_{13}} S_3(\not{k}) \Gamma_{H_{23}}] \end{aligned} \quad (18)$$

where technical details concerning the derivation of integral (18) are indicated in Appendix A.

Finally we have to specify the correlation function  $\Phi_H$  (Eq. (2) or, equivalently, the vertex function  $\tilde{\Phi}_H$  (Eq. (4), which characterize the finite size of the hadrons. Any choice for  $\tilde{\Phi}_H$  is appropriate as long as it falls off sufficiently fast in the ultraviolet region of Euclidean space to render the Feynman diagrams ultraviolet finite. We employ a Gaussian for the vertex function  $\tilde{\Phi}_H(k_E^2) \doteq \exp(-k_E^2/\Lambda_H^2)$ , where  $k_E$  is an Euclidean momentum. The size parameters  $\Lambda_H^2$  are determined by fitting to experimental data, when available, or to lattice results for the leptonic decay constants  $f_P$  where  $P = \pi, D, B$ . The leptonic decay constant  $f_P \doteq \mathcal{F}_P(M_P^2)$  is determined from [21]

$$\mathcal{F}_P(p^2) p^\mu = \frac{3g_P}{4\pi^2} \int \frac{d^4 k}{4\pi^2 i} \tilde{\Phi}_P(-k^2) \text{tr} \left[ O^\mu S_1(\not{k} + w_{21} \not{p}) \gamma^5 S_2(\not{k} - w_{12} \not{p}) \right]. \quad (19)$$

To reduce the set of values for  $\Lambda_H$ , we use a unified size parameter for hadrons with the same flavor content. The best fit to the decay constants  $f_P$  is obtained (see Table I) when the values of the constituent quark masses and the parameters  $\Lambda_H$  are chosen as follows [21]

$$\begin{array}{cccccc} m_{u(d)} & m_s & m_c & m_b & & \\ \hline 0.235 & 0.333 & 1.67 & 5.06 & & \text{GeV} \end{array} \quad (20)$$

and

$$\begin{array}{cccccc} \Lambda_{\pi(\sigma)} & \Lambda_K & \Lambda_D & \Lambda_B & & \\ \hline 1 & 1.6 & 2 & 2.25 & & \text{GeV} \end{array} \quad (21)$$

With the hadron parameters fixed, from Eq. (8), which was set up in the context of a linear realization of chiral symmetry, we deduce a  $\sigma$  mass of

$$M_\sigma = 385.4 \text{ MeV} . \quad (22)$$

The predicted value we obtain is close to the BES result [13] of  $M_\sigma = 390_{-36}^{+60}$  MeV, which sets the lower scale for the range of mass values compiled in [1].

### III. ELECTROMAGNETIC PROPERTIES OF $\pi$ AND $\sigma$

In this section we proceed with the formalism on the electromagnetic properties of  $\pi$  and  $\sigma$  mesons. For consistency we also include the  $\pi$  meson in the discussion, where, in addition, the model predictions will serve to solidify the validity of the previously outlined approach. In the analysis we consider the following related processes: the electromagnetic transition of charged pions, that is  $\pi^\pm \rightarrow \pi^\pm \gamma$ , and the form factors characterizing the anomaly transitions  $\pi^0 \rightarrow \gamma\gamma$  and  $\sigma \rightarrow \gamma\gamma$  for different kinematical regimes of the photons (real and virtual) All amplitudes considered are obtained in a manifestly gauge-invariant form.

When gauging (11) the nonlocal strong interaction Lagrangian  $\mathcal{L}_{\text{int}}^{\text{Str}}$ , additional "contact" vertices are generated, which couple hadrons, quarks and photons, as already discussed in Sec. II. In particular, for the process  $\pi^\pm \rightarrow \pi^\pm \gamma$  we need a vertex describing the coupling of a charged pion, a single photon and two quarks (Fig.3a). The coupling of  $\sigma$  to a photon and two quarks (Fig.3a) and to two photons and two quarks (Fig.3b) will contribute to the transition  $\sigma \rightarrow \gamma\gamma$ .

The full set of Feynman diagrams for the electromagnetic transition amplitudes considered are summarized in the following: The transition  $\pi^\pm \rightarrow \pi^\pm \gamma$  is described by a triangle diagram (Fig.4a) and the two additional contact diagrams of Figs.4b and 4c. The process  $\pi^0 \rightarrow \gamma\gamma$  obtains a contribution by the single diagram of Fig.5a. The transition amplitude  $\sigma \rightarrow \gamma\gamma$  is generated by the four diagrams of Fig.5: a triangle diagram (Fig.5a) and three contact diagrams (Figs.5b-d). In the following we denote diagrams containing a contact vertex with a single photon line (Figs.4b, 4c, 5b and 5c) as "bubble"-diagrams and the amplitude of Fig.5d as "tadpole"-diagram. The dominant contribution to the electromagnetic form factors arises from the leading triangle diagrams (Fig.4a and 5a). We will demonstrate that diagrams containing contact vertices give negligible contribution, but in general they should be kept to guarantee electromagnetic gauge invariance. Feynman rules for the evaluation of the nonlocal vertices of Figs.3a and 3b are derived in Appendix B. Next we will give the definition of the amplitudes for the processes  $\pi^\pm \rightarrow \pi^\pm \gamma$ ,  $\pi^0 \rightarrow \gamma\gamma$  and  $\sigma \rightarrow \gamma\gamma$  and discuss the properties of the relevant form factors.

#### A. The electromagnetic form factor $F_\pi(Q^2)$ of the pion

It is convenient to write down the vertex function for the transition  $\pi^\pm(p) \rightarrow \pi^\pm(p') + \gamma(q)$  in the form

$$\Lambda^\mu(p, p') = \frac{q^\mu}{q^2} [\tilde{\Sigma}_\pi(p^2) - \tilde{\Sigma}_\pi(p'^2)] + \Lambda_\perp^\mu(p, p') \quad (23)$$

from which the Ward-Takahashi identity follows immediately

$$q_\mu \Lambda^\mu(p, p') = \tilde{\Sigma}_\pi(p^2) - \tilde{\Sigma}_\pi(p'^2). \quad (24)$$

For setting up the electromagnetic vertex function of Eq. (23) we use the pion mass operator  $\tilde{\Sigma}_\pi(p^2)$  with

$$\begin{aligned}\tilde{\Sigma}_\pi(p^2) &\doteq \frac{3g^2}{4\pi^2} \tilde{\Pi}_\pi(p^2), \\ \tilde{\Pi}_\pi(p^2) &= \int \frac{d^4k}{4\pi^2 i} \tilde{\Phi}(-k^2) D(p), \quad D(p) = \text{tr} \left[ \gamma^5 S(k + \frac{p}{2}) \gamma^5 S(k + \frac{p}{2}) \right]\end{aligned}\tag{25}$$

and  $\Lambda_\perp^\mu(p, p')$  is the part which is orthogonal to the photon momentum:  $q_\mu \Lambda_\perp^\mu(p, p') = 0$ . The explicit expression for  $\Lambda_\perp^\mu(p, p')$  results from the sum of the gauge-invariant parts of the triangle ( $\Delta$ ) (Fig.4a) and of the bubble (bub) diagrams (Figs.4b and 4c):

$$\Lambda_\perp^\mu(p, p') = \Lambda_{\Delta_\perp}^\mu(p, p') + \Lambda_{\text{bub}_\perp}^\mu(p, p'); \quad \Lambda_{\Delta_\perp(\text{bub}_\perp)}^\mu(p, p') = \frac{3g^2}{4\pi^2} I_{\Delta_\perp(\text{bub}_\perp)}^\mu(p, p'). \tag{26}$$

The separate contributions  $I_{\Delta_\perp}^\mu(p, p')$  and  $I_{\text{bub}_\perp}^\mu(p, p')$  are given by

$$\begin{aligned}I_{\Delta_\perp}^\mu(p, p') &= \int \frac{d^4k}{4\pi^2 i} \tilde{\Phi} \left( - \left[ k + \frac{p}{2} \right]^2 \right) \tilde{\Phi} \left( - \left[ k + \frac{p'}{2} \right]^2 \right) \text{tr} [\gamma^5 S(k + p') \gamma_{\perp; q}^\mu S(k + p) \gamma^5 S(k)], \\ I_{\text{bub}_\perp}^\mu(p, p') &= \frac{\eta^\mu}{\eta^2} \int \frac{d^4k}{4\pi^2 i} \tilde{\Phi}(-k^2) \int_0^1 dt \tilde{\Phi}' \left( -k^2 - t \left[ kq + \frac{q^2}{4} \right] \right) k\eta \left\{ D(p) - D(p') \right\}.\end{aligned}\tag{27}$$

where  $\tilde{\Phi}'(z) = \partial \tilde{\Phi}(z) / \partial z$ . Also,  $\gamma_{\perp; q}^\mu = \gamma^\mu - q^\mu \not{q} / q^2$  and  $\eta^\mu = P^\mu - (Pq/q^2)q^\mu$  are orthogonal to the momentum transfer  $q$  with  $P = p + p'$ .

In the limit  $q = 0$  we obtain

$$\Lambda^\mu(p, p) = \frac{\partial \tilde{\Sigma}_\pi(p^2)}{\partial p^\mu} = 2p^\mu \frac{\partial \tilde{\Sigma}_\pi(p^2)}{\partial p^2}, \tag{28}$$

while, by definition, we also have

$$\Lambda^\mu(p, p) = 2p^\mu F_\pi(0) \tag{29}$$

where  $F_\pi(0)$  is the pion charge form factor at the origin. From the comparison of Eqs. (28) and (29) it follows that the compositeness condition (3) is equivalent to the normalization of the pion form factor at the origin with  $F_\pi(0) = 1$ .

The full electromagnetic form factor  $F_\pi(Q^2)$  of the pion is defined by

$$\Lambda^\mu(p, p') \Big|_{p^2=p'^2=M_\pi^2} = P^\mu F_\pi(Q^2) \tag{30}$$

where  $Q^2 = -q^2 = -(p - p')^2$  is the Euclidean momentum transfer squared. The electromagnetic radius of the pion, related to the slope of  $F_\pi(Q^2)$  at the origin, is then given by

$$\langle r_\pi^2 \rangle = -6 \frac{dF_\pi(Q^2)}{dQ^2} \Big|_{Q^2=0}. \tag{31}$$

## B. Anomaly transitions $\pi^0 \rightarrow \gamma\gamma$ and $\sigma \rightarrow \gamma\gamma$

Anomaly processes, e.g. the decay of the neutral pion into two photons, have attracted a lot of interest, since their study helps to understand the nature of spontaneously broken symmetries. In the case of the  $\pi^0\gamma\gamma$  anomaly (known as the Adler-Bell-Jackiw anomaly [32]) the divergence of the axial-vector current (PCAC) has to be modified for the neutral pion. The evaluation of anomalies is sensitive to the regularization scheme applied to the divergent Feynman integrals. According to the Sutherland-Veltman theorem [33] there is a unique value for the axial anomaly consistent with gauge invariance. Therefore, in the study of anomalies one should use gauge-invariant regularizations, e.g., the dimensional t'Hooft-Veltman [34] or the invariant Pauli-Villars-Gupta [35,36] regularizations. Another interesting anomaly process is the two-photon decay of the scalar meson  $\sigma \rightarrow \gamma\gamma$ . This anomaly encodes the coupling of the scalar field to a pair of photons which cannot be generated in the standard way (e.g., via minimal substitution). It has microscopic nature and appears for example by calculating the corresponding quark diagram. Even if the light ( $q\bar{q}$ ) scalar meson does not exist at all, there is certain academical interest to pin down the scalar-vector-vector anomaly diagram and to study its asymptotical behavior for large photon virtualities.

The matrix elements which describe the transitions  $\pi^0 \rightarrow \gamma\gamma$  and  $\sigma \rightarrow \gamma\gamma$  can be written in general in the manifestly gauge-invariant form

$$M_{\pi^0 \rightarrow \gamma\gamma}^{\mu\nu}(q_1, q_2) = e^2 a^{\mu\nu} F_{\pi\gamma\gamma}(p^2, q_1^2, q_2^2), \quad (32)$$

$$M_{\sigma \rightarrow \gamma\gamma}^{\mu\nu}(q_1, q_2) = e^2 \left\{ b^{\mu\nu} F_{\sigma\gamma\gamma}(p^2, q_1^2, q_2^2) + c^{\mu\nu} G_{\sigma\gamma\gamma}(p^2, q_1^2, q_2^2) \right\}. \quad (33)$$

The tensors  $a^{\mu\nu}$ ,  $b^{\mu\nu}$  and  $c^{\mu\nu}$  refer to the Lorentz structures:

$$\begin{aligned} a^{\mu\nu} &= \epsilon^{\mu\nu\alpha\beta} (q_1)_\alpha (q_2)_\beta, \\ b^{\mu\nu} &= g^{\mu\nu} (q_1 q_2) - q_1^\nu q_2^\mu, \\ c^{\mu\nu} &= g^{\mu\nu} q_1^2 q_2^2 + q_1^\mu q_2^\nu (q_1 q_2) - q_1^\mu q_1^\nu q_2^2 - q_2^\mu q_2^\nu q_1^2, \end{aligned} \quad (34)$$

while  $q_1$  and  $q_2$  are the photon four-momenta and  $p = q_1 + q_2$  is the meson momentum. Here,  $F_{\pi\gamma\gamma}(p^2, q_1^2, q_2^2)$  is the axial anomaly form factor. The scalar anomaly is characterized by two form factors:  $F_{\sigma\gamma\gamma}(p^2, q_1^2, q_2^2)$  and  $G_{\sigma\gamma\gamma}(p^2, q_1^2, q_2^2)$ . Usually only one of the form factors, that is  $F_{\sigma\gamma\gamma}$ , is discussed in the literature. However, when both photons are off-shell, constraints set by gauge invariance result in the two terms of the matrix element  $M_{\sigma \rightarrow \gamma\gamma}^{\mu\nu}$ , proportional to the Lorentz structures  $b^{\mu\nu}$  and  $c^{\mu\nu}$ . If at least one of the photons is real, then only the first form factor  $F_{\sigma\gamma\gamma}$  gives a non-vanishing contribution to the invariant matrix element. The decay width of the transition  $H \rightarrow \gamma\gamma$  with  $H = \pi$  or  $\sigma$  is given by

$$\Gamma_{H\gamma\gamma} = \frac{\pi}{4} \alpha^2 M_H^3 g_{H\gamma\gamma}^2 \quad (35)$$

where  $g_{H\gamma\gamma} = F_{H\gamma\gamma}(M_H^2, 0, 0)$  is the anomaly coupling constant and  $\alpha = e^2/(4\pi)$ .

For the evaluation of the anomaly form factors, both for  $\pi$  and  $\sigma$ , we pursue the following strategy. First we consider the calculation of the anomaly form factors  $F_{\pi\gamma\gamma}(p^2, q_1^2, q_2^2)$ ,  $F_{\sigma\gamma\gamma}(p^2, q_1^2, q_2^2)$  and  $G_{\sigma\gamma\gamma}(p^2, q_1^2, q_2^2)$  in so-called local limit. In this case the dimensional parameter  $\Lambda_\pi$ , appearing in the  $\pi(\sigma)$  meson vertex function  $\tilde{\Phi}(-k^2)$ , is taken to infinity or,

which is equivalent,  $\tilde{\Phi}(-k^2) \rightarrow 1$ . We obtain analytical expressions for the anomaly form factors and show that for the case of  $\pi^0 \rightarrow \gamma\gamma^*$  the form factor has the incorrect behavior for large photon virtualities in the Euclidean region. Then we repeat the derivation using the nonlocal approach and show that the correct asymptotics for the  $\pi\gamma\gamma^*$  form factor can be reproduced when using the mesonic quark-antiquark wave function. The final numerical analysis for the complete form factors will be done in a separate section.

### 1. Local $\pi^0\gamma\gamma$ and $\sigma\gamma\gamma$ diagrams

The Feynman integral corresponding to the local (L) anomalous triangle diagram is written as

$$I_{\Delta,L}^{\mu\nu;M}(q_1, q_2) = \int \frac{d^4k}{4\pi^2 i} \text{tr} \left\{ \gamma^\mu S(\not{k} + \not{q}_1) \Gamma_M(\not{k} - \not{q}_2) \gamma^\nu S(\not{k}) \right\} \quad (36)$$

where  $\Gamma_\pi = i\gamma^5$  for  $\pi$  and  $\Gamma_\sigma = I$  for  $\sigma$ . For simplicity we drop a common factor of  $-3/4\pi^2$ . The complete anomaly integral (36) is free of the logarithmic ultraviolet (UV) divergence. Separate contributions to Eq. (36) with the UV divergences are treated using dimensional regularization [34]. In this case we use the definition for  $\gamma^5$  in D dimensions (see details in [37]) to guarantee the fulfilment of two important properties:  $(\gamma^5)^2 = I$  and  $\text{tr}(\gamma^5\gamma^\mu\gamma^\nu) = 0$ . For the pseudoscalar anomaly the UV divergency is completely gone due to the contraction of the divergent integral with the trace  $\text{tr}(\gamma^5\gamma^\mu\gamma^\nu)$ , which by definition is zero in any dimension. In the case of the scalar anomaly ( $\sigma\gamma\gamma$  diagram) the use of the gauge-invariant regularization (e.g., dimensional regularization) guarantees the cancellation of the UV parts and generates the correct finite part. The finite part of the scalar anomaly is the same for both types of gauge-invariant regularizations. The master formulas used in dimensional regularization are

$$\begin{aligned} \text{tr}(\gamma^5\gamma^\mu\gamma^\nu) \int d^Dk \frac{k^2}{(m^2 - k^2 - D_0)^3} &= 0 && \text{(for } \pi \text{ meson)} \\ \int d^Dk \frac{4k^\mu k^\nu + g^{\mu\nu}(m^2 - k^2 - D_0)}{(m^2 - k^2 - D_0)^3} &= 0 && \text{(for } \sigma \text{ meson)} \end{aligned}$$

where  $D_0 = \alpha_1\alpha_2p^2 + \alpha_1\alpha_3q_1^2 + \alpha_2\alpha_3q_2^2$  with  $p = q_1 + q_2$  arises when using the  $\alpha$ -parametrization.

The integral Eq.(36) is gauge invariant

$$I_{\Delta,L}^{\mu\nu;\Gamma}(q_1, q_2) \cdot (q_1)_\mu = I_{\Delta,L}^{\mu\nu;\Gamma}(q_1, q_2) \cdot (q_2)_\nu = 0$$

as can be easily deduced from the Ward identity

$$S(\not{k}) \not{q}_1 S(\not{k} + \not{q}_1) = S(\not{k} + \not{q}_1) - S(\not{k})$$

and simple algebra.

The integral of Eq.(36) is particularly simple for the case of the pion with

$$I_{\Delta,L}^{\mu\nu;\pi}(q_1, q_2) = m a^{\mu\nu} F_L^\pi(p^2, q_1^2, q_2^2) \quad (37)$$

where the form factor  $F_L^\pi$  is given by the two-dimensional integral  $I_L$ :

$$F_L^\pi(p^2, q_1^2, q_2^2) \equiv I_L(p^2, q_1^2, q_2^2) = \int d^3\alpha \delta\left(1 - \sum_{i=1}^3 \alpha_i\right) \frac{1}{m^2 - D_0}. \quad (38)$$

The double integral  $I_L$  can be further reduced to a single one using the 't Hooft-Veltman technique [38] and can be finally expressed by a combination of Spence functions. Here, however, we will stay with the integral representation. We have

$$I_L(p^2, q_1^2, q_2^2) = \int_0^1 dx \left\{ \frac{\ln[1 - x(1-x)p^2/m^2]}{\lambda^{1/2} \cdot x + q_1^2 - \alpha_0 p^2} - \frac{\ln[1 - x(1-x)q_2^2/m^2]}{\lambda^{1/2} \cdot x - q_1^2 - q_2^2 \alpha_0 / (1 - \alpha_0)} + \frac{\ln[1 - x(1-x)q_1^2/m^2]}{\lambda^{1/2} \cdot x + q_1^2 (1 - \alpha_0) / \alpha_0 + q_2^2} \right\}, \quad (39)$$

where

$$\lambda \doteq \lambda(p^2, q_1^2, q_2^2) = p^4 + q_1^4 + q_2^4 - 2p^2 q_1^2 - 2p^2 q_2^2 - 2q_1^2 q_2^2 \quad (40)$$

is a kinematical triangle function and  $\alpha_0 = (p^2 + q_1^2 - q_2^2 + \lambda^{1/2})/2p^2$ . All three thresholds can be readily seen from this representation. In particular, when both photons are on their mass-shell ( $q_1^2 = q_2^2 = 0$ ) we get

$$\begin{aligned} I_L(p^2, 0, 0) &= -\frac{1}{2p^2} \int_0^1 dx \frac{\ln[1 - x(1-x)p^2/m^2]}{x(1-x)} \\ &= \frac{1}{4} \int_0^1 dv \ln\left(\frac{1 + \sqrt{1-v}}{1 - \sqrt{1-v}}\right) \cdot \frac{1}{m^2 - v \cdot p^2/4 - i\epsilon} \\ &= \int_{4m^2}^{\infty} \frac{d\kappa^2}{\kappa^2} \cdot \frac{\rho(\kappa^2)}{\kappa^2 - p^2 - i\epsilon} = \frac{2}{p^2} \left( \text{ArcSin} \left[ \sqrt{\frac{p^2}{4m^2}} \right] \right)^2, \end{aligned} \quad (41)$$

where  $\rho(\kappa^2) = \ln\left\{\left(1 + \sqrt{1 - 4m^2/\kappa^2}\right) / \left(1 - \sqrt{1 - 4m^2/\kappa^2}\right)\right\}$  is the spectral function.

Another interesting limiting case is when one of the photons has large Euclidean momentum, for instance,  $q_1^2 = -Q^2$ ,  $q_2^2 = 0$  and  $p^2 = 0$ . In the limit  $Q^2 \rightarrow \infty$  the integral Eq.(39) reduces to

$$I_L(0, -Q^2, 0) \rightarrow \frac{1}{2Q^2} \int_0^1 dx \frac{\ln[1 + x(1-x)Q^2/m^2]}{x(1-x)} \rightarrow \frac{\ln^2(Q^2/m^2)}{2Q^2}.$$

Note that such an asymptotics is in contradiction to the QCD-prediction for the  $\pi^0\gamma^*\gamma$  form factor of  $1/Q^2$  [39].

In the following we turn to the evaluation of the  $\sigma\gamma\gamma$  diagram in the local limit using dimensional regularization. The defining integral of Eq. (36) can be written as

$$I_{\Delta, L}^{\mu\nu; \sigma}(q_1, q_2) = F_L^\sigma(p^2, q_1^2, q_2^2) b^{\mu\nu} + G_L^\sigma(p^2, q_1^2, q_2^2) c^{\mu\nu}, \quad (42)$$

with

$$F_L^\sigma(p^2, q_1^2, q_2^2) = \frac{(I_{\Delta, L}^\sigma \cdot b) c^2 - (I_{\Delta, L}^\sigma \cdot c) (b \cdot c)}{b^2 c^2 - (b \cdot c)^2},$$

$$G_L^\sigma(p^2, q_1^2, q_2^2) = \frac{(I_{\Delta, L}^\sigma \cdot c) b^2 - (I_{\Delta, L}^\sigma \cdot b) (b \cdot c)}{b^2 c^2 - (b \cdot c)^2},$$
(43)

and where the dot-product refers to the contraction of the Lorentz indices.

Using the  $\alpha$ -parametrization we have

$$F_L^\sigma(p^2, q_1^2, q_2^2) = -m \int d^3\alpha \delta\left(1 - \sum_{i=1}^3 \alpha_i\right) \frac{1 - 4\alpha_1\alpha_2}{m^2 - D_0},$$

$$G_L^\sigma(p^2, q_1^2, q_2^2) = \frac{m}{q_1^2 q_2^2} \int d^3\alpha \delta\left(1 - \sum_{i=1}^3 \alpha_i\right) \frac{\alpha_1(1 - 2\alpha_1)q_1^2 + \alpha_2(1 - 2\alpha_2)q_2^2}{m^2 - D_0}.$$
(44)

Again, one integration in Eq. (44) can be performed analytically (the resulting expressions (109) and (110) are indicated in Appendix C). For the case  $q_1^2 = q_2^2 = 0$  we get

$$F_L^\sigma(p^2, 0, 0) = -\frac{m}{4} \int_0^1 dv \ln\left(\frac{1 + \sqrt{1-v}}{1 - \sqrt{1-v}}\right) \frac{1-v}{m^2 - v \cdot p^2/4},$$

$$G_L^\sigma(p^2, 0, 0) = \frac{2m}{4m^2 - p^2} \int_0^1 dv \left\{ \frac{1}{4}(1+v) \ln\left(\frac{1 + \sqrt{1-v}}{1 - \sqrt{1-v}}\right) - \sqrt{1-v} \right\} \frac{1-v}{m^2 - v \cdot p^2/4}.$$
(45)

## 2. The nonlocal $\pi^0\gamma\gamma$ and $\sigma\gamma\gamma$ diagrams

For a nontrivial, that is nonlocal, meson-quark vertex the evaluation of the relevant Feynman diagrams is based on a method outlined in [19]. This technique was originally developed to derive a representation for the  $\pi^0\gamma\gamma$  diagram (Fig.5a) with a dressed pion-quark vertex, which is described by an arbitrary function  $\tilde{\Phi}(-k^2)$  decreasing rapidly in the Euclidean region. It also preserves translational and gauge invariance in a manifest way and guarantees the fulfilment of vector and anomalous Ward identities.

In our model the  $\pi^0\gamma\gamma$  form factor is given by

$$F_{\pi\gamma\gamma}(p^2, q_1^2, q_2^2) = \frac{g}{2\pi^2\sqrt{2}} m I_{\text{NL}}(p^2, q_1^2, q_2^2)$$
(46)

where  $I_{\text{NL}}$  is the nonlocal (NL) quark-loop integral:

$$I_{\text{NL}}(p^2, q_1^2, q_2^2) = \int \frac{d^4k}{4\pi^2 i} \frac{\tilde{\Phi}(-k^2)}{[m^2 - (k + p/2)^2] [m^2 - (k - p/2)^2] [m^2 - (k + q/2)^2]}$$

$$= \int_0^\infty dt \left(\frac{t}{1+t}\right)^2 \int d^3\alpha \delta\left(1 - \sum_{i=1}^3 \alpha_i\right) \cdot \{-\tilde{\Phi}'(z)\}$$
(47)

with  $q = q_2 - q_1$ .

The argument  $z$  appearing in the vertex function is written in the form

$$\begin{aligned} z &= \frac{t^2}{1+t} D + \frac{t}{1+t} \Delta, \\ D &= m^2 - \alpha_1 \alpha_2 p^2 - \alpha_1 \alpha_3 q_1^2 - \alpha_2 \alpha_3 q_2^2 \equiv m^2 - D_0, \\ \Delta &= m^2 - \frac{p^2}{4} + \frac{\alpha_3}{2} (p^2 - q_1^2 - q_2^2). \end{aligned}$$

We choose to define the functional dependence of the vertex function as  $\tilde{\Phi}(-k^2)$ , hence after transition to the Euclidean region ( $k^0 \rightarrow ik_4$  or  $k^2 \rightarrow -k_E^2$ ) the argument changes sign. This convention allows a consistent choice of the functional form for  $\tilde{\Phi}(k_E^2)$  in the Euclidean region, where we finally perform the integrations. For example, particular forms of the vertex function are  $\tilde{\Phi}(k_E^2) = \exp(-k_E^2/\Lambda^2)$  (Gaussian vertex function) or  $\tilde{\Phi}(k_E^2) = 1/(1 + k_E^2/\Lambda^2)^n$  (pole vertex function), where  $1/\Lambda$  characterizes the size of the meson. Obviously, the limiting local case  $I_{\text{NL}} \rightarrow I_L$  can be recovered for  $\Lambda \rightarrow \infty$ . This limit also serves as a check for the numerical calculations used in the final step of the evaluation. The following analytical results are obtained for an arbitrary form of  $\tilde{\Phi}(-k^2)$ . Only when turning to the final numerical calculation, a specific form of  $\tilde{\Phi}(k_E^2)$  (Gaussian vertex function) will be used.

Again, one integration in Eq. (47) is performed by linearization of the argument  $z$  with respect to one of the  $\alpha$  parameters as it was done in the local case. The resulting expressions are indicated in Appendix D, as given by Eqs. (112) and (113). For the study of the dependence of the  $\pi\gamma\gamma$  form factor on the photon virtualities in the Euclidean region it is useful to introduce the variables:  $q_1^2 = -(1+\omega)Q^2/2$  and  $q_2^2 = -(1-\omega)Q^2/2$  where  $Q^2$  and  $\omega$  are the total virtuality and the asymmetry, respectively<sup>1</sup>. With this convention we define the pion form factor as

$$F_{\pi\gamma^*\gamma^*}(Q^2, \omega) \doteq F_{\pi\gamma\gamma}\left(M_\pi^2, -(1+\omega)\frac{Q^2}{2}, -(1-\omega)\frac{Q^2}{2}\right). \quad (48)$$

The particular choice  $\omega = \pm 1$  corresponds to the physically interesting case where one of the photons is virtual and the other is on its mass-shell. The corresponding transition form factor  $F_{\pi\gamma\gamma^*}(Q^2) \doteq F_{\pi\gamma\gamma}(M_\pi^2, -Q^2, 0)$  has recently been measured by the CLEO Collaboration [40] for momentum transfers in the range from 1.5 to 9 GeV<sup>2</sup>. A discussion of previous experiments can also be found in Ref. [40]. The CLEO data confirmed the predictions of perturbative QCD (pQCD) [39] for the asymptotic behavior of  $F_{\pi\gamma\gamma^*}(Q^2)$  at large  $Q^2$ :

$$F_{\pi\gamma\gamma^*}(Q^2) = \frac{2F_\pi}{Q^2} + O\left(\frac{1}{Q^4}\right) \quad (49)$$

where  $F_\pi = f_\pi/\sqrt{2}$ .

A detailed analysis of the different QCD approaches to the  $F_{\pi\gamma\gamma^*}(Q^2)$  form factor has recently been done in [41]. Unfortunately, a straightforward calculation of  $F_{\pi\gamma\gamma^*}(Q^2)$  in the

---

<sup>1</sup>Another possibility is to work in terms of the average virtuality. In this case the variable  $Q^2$  should be rescaled as  $Q^2 \rightarrow 2Q^2$  in all further formulas.

context of QCD is either not fully possible, because the operator product expansion (OPE) fails at small  $Q^2$ , or contains unknown parameters like the twist-four scale parameter  $\delta^2$  related to the gluon condensate [42,43]. Therefore, an analysis of  $F_{\pi\gamma\gamma^*}$  in our QCD-motivated approach seems to be quite reasonable. Information about the anomaly form factors for non-trivial photon virtualities is relevant to forthcoming experiments on production of pseudoscalar mesons in  $\gamma^*\gamma^*$  collisions. Also, there is the project to search for a light scalar meson in very peripheral heavy ion collisions (for a recent review see Ref. [44]).

For the analysis of  $F_{\pi\gamma^*\gamma^*}$  we perform a systematic expansion in powers of  $1/Q^2$  including leading order (LO) and next-to-leading order (NLO) terms with

$$F_{\pi\gamma^*\gamma^*}(Q^2, \omega) = 2F_\pi \left\{ \frac{J_\pi^{\text{LO}}(\omega)}{Q^2} + \frac{J_\pi^{\text{NLO}}(\omega)}{Q^4} + O\left(\frac{1}{Q^6}\right) \right\}. \quad (50)$$

The expansion coefficients  $J_\pi^{\text{LO}}(\omega)$  and  $J_\pi^{\text{NLO}}(\omega)$  are given in our approach by

$$J_\pi^{\text{LO}}(\omega) = \frac{2}{3} \frac{R_\pi^{\text{LO}}(\omega)}{R_\pi^{\text{LO}}(0)}, \quad J_\pi^{\text{NLO}}(\omega) = \frac{2}{3} \frac{R_\pi^{\text{NLO}}(\omega)}{R_\pi^{\text{LO}}(0)}. \quad (51)$$

The structure integrals  $R_\pi^{\text{LO}}(\omega)$  and  $R_\pi^{\text{NLO}}(\omega)$  are derived in Appendix D applying the chiral limit with  $M_\pi^2 = 0$  and are written as

$$R_\pi^{\text{LO}}(\omega) = \frac{1}{\omega} \int_0^\infty \frac{dt}{t+1} \tilde{\Phi}(m^2 t) \text{Ln}_-(t, \omega), \quad R_\pi^{\text{NLO}}(\omega) = -4m^2 \int_0^\infty dt \tilde{\Phi}(m^2 t) D(t, \omega), \quad (52)$$

where

$$\begin{aligned} \text{Ln}_\pm(t, \omega) &\doteq \ln \left[ \frac{1+t(1+\omega)}{1+t} \right] \pm \ln \left[ \frac{1+t(1-\omega)}{1+t} \right], \\ D(t, \omega) &\doteq \frac{t}{[1+t(1+\omega)][1+t(1-\omega)]}. \end{aligned}$$

In the derivation of Eqs. (50) and (51) we use the identity

$$F_\pi = \frac{3g}{8\pi^2\sqrt{2}} R_\pi^{\text{LO}}(0), \quad (53)$$

relating  $F_\pi$  and the meson-quark coupling constant  $g$ . From the expressions of Eq. (52) it can be readily seen that the expansion coefficients contain only even powers of  $\omega$ , which is a consequence of Bose-Einstein symmetry and charge conjugation invariance.

At this stage of the development we indicate a first comparison of our results for the expansion coefficients calculated at  $\omega = 1$  and  $\omega = 0$  to the ones predicted by pQCD [39,42,43]. A summary of previous model results for  $J_\pi^{\text{LO}}(1)$  and  $J_\pi^{\text{LO}}(0)$  can be found in Ref. [45]. First, we consider the experimentally accessible case  $w = \pm 1$ , where one of the photons is real and the other one is virtual. Our numerical result for  $J_\pi^{\text{LO}}(1) = 0.998 \simeq 1$  is in very good agreement with the pQCD prediction of  $J_\pi^{\text{LO}}(1) \equiv 1$  [39]. In the relativistic quark model the NLO coefficient  $J_\pi^{\text{NLO}}(1)$  is proportional to the constituent quark mass squared and results in  $J_\pi^{\text{NLO}}(1) = -0.37 \text{ GeV}^2$ . The pQCD approach predicts [41]

$$J_{\pi}^{\text{NLO}}(1) = -\frac{80}{27}\delta^2, \quad (54)$$

where  $\delta^2$  is the twist-four scale parameter related to the gluon condensate [42,43]. Originally, this quantity was estimated to have a value of  $\delta^2 = (0.2 \pm 0.02) \text{ GeV}^2$  using the QCD sum rule approach [43]. A recent evaluation [41] results in:  $\delta^2 = (0.19 \pm 0.02) \text{ GeV}^2$ . By taking into account the value of Ref. [43] the pQCD prediction is

$$J_{\pi}^{\text{NLO}}(1) = -(0.59 \pm 0.06) \text{ GeV}^2. \quad (55)$$

Now we turn to the case  $\omega = 0$ . We exactly reproduce the LO coefficient predicted by pQCD [43]:  $J_{\pi}^{\text{LO}}(0) = 2/3$ . For the NLO coefficient our result is

$$J_{\pi}^{\text{NLO}}(0) = -\frac{4}{3}m^2 = -0.074 \text{ at } m = 235 \text{ MeV}. \quad (56)$$

The result of pQCD is again proportional to  $\delta^2$  [43]:

$$J_{\pi}^{\text{NLO}}(0) = -\frac{32}{27}\delta^2 = -(0.24 \pm 0.02) \text{ GeV}^2. \quad (57)$$

From this comparison we conclude that our prediction for the LO expansion coefficients  $J_{\pi}^{\text{LO}}(1)$  and  $J_{\pi}^{\text{LO}}(0)$  are in perfect agreement with the expectation of pQCD. The NLO coefficients are rather sensitive to the choice of the constituent quark mass. In particular, when using  $m = 395 \text{ MeV}$  in the calculation of  $J_{\pi}^{\text{NLO}}(1)$  and  $m = 420 \text{ MeV}$  in the case of  $J_{\pi}^{\text{NLO}}(0)$  the central values of the NLO coefficients predicted by pQCD can be fitted.

For the process  $\sigma \rightarrow \gamma\gamma$  we have to evaluate, in addition to the triangle diagram (Fig.5a), the bubble (Figs.5b and 5c) and tadpole diagrams (Fig.5d), which arise from gauging the nonlocal  $\sigma q\bar{q}$  interaction Lagrangian. Each particular diagram is not gauge invariant by itself, but the total sum fulfills the gauge invariance requirement. To simplify the calculation we split the contribution of each diagram into a part which is gauge invariant and one which is not. This separation can be achieved in the following manner. For the  $\gamma$ -matrices and vectors with open Lorentz indices  $\mu$  and  $\nu$  we use the representation:

$$\begin{aligned} \gamma^{\mu} &= \gamma_{\perp; q_1}^{\mu} + q_1^{\mu} \frac{\not{q}_1}{q_1^2}, & v^{\mu} &= v_{\perp; q_1}^{\mu} + q_1^{\mu} \frac{v q_1}{q_1^2}, \\ \gamma^{\nu} &= \gamma_{\perp; q_2}^{\nu} + q_2^{\nu} \frac{\not{q}_2}{q_2^2}, & v^{\nu} &= v_{\perp; q_2}^{\nu} + q_2^{\nu} \frac{v q_2}{q_2^2}, \end{aligned} \quad (58)$$

such that  $\gamma_{\perp; q_1}^{\mu}(q_1)_{\mu} = v_{\perp; q_1}^{\mu}(q_1)_{\mu} = 0$  and  $\gamma_{\perp; q_2}^{\nu}(q_2)_{\nu} = v_{\perp; q_2}^{\nu}(q_2)_{\nu} = 0$ . Expressions for diagrams containing only  $\perp$ -values are gauge invariant separately. It is easy to show that the remaining terms, which are not gauge invariant, cancel each other in total.

The gauge-invariant parts of the nonlocal  $\sigma\gamma\gamma$ -triangle ( $\Delta$ ), bubble (bub) and tadpole (tad) diagrams are given by

$$I_{\Delta\perp}^{\mu\nu}(q_1, q_2) = \int \frac{d^4k}{4i\pi^2} \tilde{\Phi}(-k^2) \text{tr} \left\{ \gamma_{\perp; q_1}^{\mu} S\left(k + \frac{\not{p}}{2}\right) S\left(k - \frac{\not{p}}{2}\right) \gamma_{\perp; q_2}^{\nu} S\left(k + \frac{\not{q}}{2}\right) \right\}$$

$$= F_{\Delta_{\perp}}^{\sigma}(p^2, q_1^2, q_2^2) b^{\mu\nu} + G_{\Delta_{\perp}}^{\sigma}(p^2, q_1^2, q_2^2) c^{\mu\nu}, \quad (59)$$

$$I_{\text{bub}_{\perp}}^{\mu\nu}(q_1, q_2) = - \int \frac{d^4 k}{4\pi^2 i} \int_0^1 d\tau \tilde{\Phi}'(-x(0, q_2)) \left\{ k_{\perp; q_2}^{\nu} \text{tr} \left[ \gamma_{\perp; q_1}^{\mu} S(k + q_1/2) S(k - q_1/2) \right] \right\} \\ + (q_1 \leftrightarrow q_2, \mu \leftrightarrow \nu) = F_{\text{bub}_{\perp}}^{\sigma}(p^2, q_1^2, q_2^2) b^{\mu\nu} + G_{\text{bub}_{\perp}}^{\sigma}(p^2, q_1^2, q_2^2) c^{\mu\nu}, \quad (60)$$

$$I_{\text{tad}_{\perp}}^{\mu\nu}(q_1, q_2) = \int \frac{d^4 k}{4\pi^2 i} \text{tr} [S(k)] \int_0^1 d\tau \left[ - \frac{c^{\mu\nu}}{4 q_1^2 q_2^2} \cdot \left\{ \tilde{\Phi}'(-x(0, p)) + \tilde{\Phi}'(-x(0, q)) \right\} \right] \\ + \tau \int_0^1 dl \left( k + \frac{q_2}{2} \right)_{\perp; q_1}^{\mu} k_{\perp; q_2}^{\nu} \left\{ \tilde{\Phi}''(-x(q_1, q_2)) + \tilde{\Phi}''(-x(-q_1, q_2)) \right\} \\ + (q_1 \leftrightarrow q_2, \mu \leftrightarrow \nu) = F_{\text{tad}_{\perp}}^{\sigma}(p^2, q_1^2, q_2^2) b^{\mu\nu} + G_{\text{tad}_{\perp}}^{\sigma}(p^2, q_1^2, q_2^2) c^{\mu\nu}, \quad (61)$$

where

$$x(q_1, q_2) = k^2 + k\tau(l q_1 + q_2) + \frac{\tau}{4}(l q_1^2 + 2 l q_1 q_2 + q_2^2).$$

Applying the  $\alpha$ -parametrization for the gauge-invariant part of the triangle diagram gives

$$F_{\Delta_{\perp}}^{\sigma} = -m \int_0^{\infty} dt \frac{t^3}{(1+t)^4} \int d^3 \alpha \delta \left( 1 - \sum_{i=1}^3 \alpha_i \right) \left\{ -\tilde{\Phi}'(z) \right\} [t(1 - 4\alpha_1 \alpha_2) + 2\alpha_3], \quad (62)$$

$$G_{\Delta_{\perp}}^{\sigma} = - \frac{m}{q_1^2 q_2^2} \int_0^{\infty} dt \frac{t^2}{(1+t)^2} \int d^3 \alpha \delta \left( 1 - \sum_{i=1}^3 \alpha_i \right) \left\{ -\tilde{\Phi}'(z) \right\} \\ \times \left\{ -m^2 + \frac{(1 + 2\alpha_1 t)(1 + 2\alpha_2 t)}{4(1+t)^2} p^2 + \frac{t(\alpha_1 - \alpha_2)}{2(1+t)^2} \left( (1 + 2\alpha_1 t) q_1^2 - (1 + 2\alpha_2 t) q_2^2 \right) \right\}. \quad (63)$$

Again, using the t'Hooft-Veltman technique one integration in Eqs. (62) and (63) can be performed. The resulting expressions are indicated in Eqs. (120) and (121) of Appendix E. The analytical results for the form factors  $F(G)_{\text{bub}_{\perp}}^{\sigma}$  and  $F(G)_{\text{tad}_{\perp}}^{\sigma}$  are given in Appendix F (Eqs. (128)-(131)).

In the local limit, that is  $\Lambda \rightarrow \infty$ , we obtain

$$F_{\Delta_{\perp}}^{\sigma} \rightarrow F_{\text{L}}^{\sigma}, \quad F_{\text{bub}_{\perp}}^{\sigma} \rightarrow 0, \quad F_{\text{tad}_{\perp}}^{\sigma} \rightarrow 0, \\ G_{\Delta_{\perp}}^{\sigma} \rightarrow G_{\text{L}}^{\sigma} + \frac{m}{2 q_1^2 q_2^2}, \quad G_{\text{bub}_{\perp}}^{\sigma} \rightarrow -\frac{m}{q_1^2 q_2^2}, \quad G_{\text{tad}_{\perp}}^{\sigma} \rightarrow \frac{m}{2 q_1^2 q_2^2}.$$

We therefore recover the local  $\sigma\gamma\gamma$  form factors:

$$F_{\text{NL}}^{\sigma} = F_{\Delta_{\perp}}^{\sigma} + F_{\text{bub}_{\perp}}^{\sigma} + F_{\text{tad}_{\perp}}^{\sigma} \rightarrow F_{\text{L}}^{\sigma}, \\ G_{\text{NL}}^{\sigma} = G_{\Delta_{\perp}}^{\sigma} + G_{\text{bub}_{\perp}}^{\sigma} + G_{\text{tad}_{\perp}}^{\sigma} \rightarrow G_{\text{L}}^{\sigma},$$

which were already indicated in Eq. (44).

The anomaly form factors  $F_{\sigma\gamma\gamma}$  and  $G_{\sigma\gamma\gamma}$  are expressed in terms of the functions introduced above as

$$F_{\sigma\gamma\gamma}(p^2, q_1^2, q_2^2) = -\frac{5g}{6\pi^2\sqrt{2}} \left[ F_{\Delta\perp}^\sigma(p^2, q_1^2, q_2^2) + F_{\text{bub}\perp}^\sigma(p^2, q_1^2, q_2^2) + F_{\text{tad}\perp}^\sigma(p^2, q_1^2, q_2^2) \right], \quad (64)$$

$$G_{\sigma\gamma\gamma}(p^2, q_1^2, q_2^2) = -\frac{5g}{6\pi^2\sqrt{2}} \left[ G_{\Delta\perp}^\sigma(p^2, q_1^2, q_2^2) + G_{\text{bub}\perp}^\sigma(p^2, q_1^2, q_2^2) + G_{\text{tad}\perp}^\sigma(p^2, q_1^2, q_2^2) \right]. \quad (65)$$

In analogy to the case of the pion we define the  $\sigma\gamma\gamma$  form factors using the  $Q^2$  and  $\omega$  variables accordingly:

$$F_{\sigma\gamma^*\gamma^*}(Q^2, \omega) \doteq F_{\sigma\gamma\gamma} \left( M_\sigma^2, -(1+\omega)\frac{Q^2}{2}, -(1-\omega)\frac{Q^2}{2} \right), \quad (66)$$

$$G_{\sigma\gamma^*\gamma^*}(Q^2, \omega) \doteq G_{\sigma\gamma\gamma} \left( M_\sigma^2, -(1+\omega)\frac{Q^2}{2}, -(1-\omega)\frac{Q^2}{2} \right). \quad (67)$$

The final numerical analysis indicates that the additional nonlocal diagrams (bubble and tadpole) are significantly suppressed. For simplicity below we discuss the power expansion for  $F_{\sigma\gamma^*\gamma^*}(Q^2, \omega)$  and  $G_{\sigma\gamma^*\gamma^*}(Q^2, \omega)$  in the limit  $M_\sigma^2 = 0$ , where only the gauge-invariant part of the triangle diagram is included. In the numerical analysis (Sec. V) we will take into account all diagrams and use the value of  $M_\sigma = 385.4$  MeV as predicted by our approach. For the power expansion of the  $\sigma\gamma\gamma$  form factor we pull out, with the help of Eq. (53), a common scaling factor  $2F_\pi$ :

$$F_{\sigma\gamma^*\gamma^*}(Q^2, \omega) = 2F_\pi \left\{ \frac{J_\sigma^{\text{LO}}(\omega)}{Q^2} + \frac{J_\sigma^{\text{NLO}}(\omega)}{Q^4} + O\left(\frac{1}{Q^6}\right) \right\}, \quad (68)$$

$$G_{\sigma\gamma^*\gamma^*}(Q^2, \omega) = 2F_\pi \left\{ \frac{K_\sigma^{\text{LO}}(\omega)}{Q^4} + \frac{K_\sigma^{\text{NLO}}(\omega)}{Q^6} + O\left(\frac{1}{Q^8}\right) \right\}.$$

The expansion coefficients  $J_\sigma^{\text{LO}}(\omega)$ ,  $J_\sigma^{\text{NLO}}(\omega)$ ,  $K_\sigma^{\text{LO}}(\omega)$  and  $K_\sigma^{\text{NLO}}(\omega)$  are derived in the limit indicated above as

$$J_\sigma^{\text{LO}}(\omega) = \frac{5}{3\omega^2} \left\{ J_\pi^{\text{LO}}(\omega) - \frac{2}{3} \right\}, \quad J_\sigma^{\text{NLO}}(\omega) = \frac{10}{9} \frac{R_{\sigma 1}^{\text{NLO}}(\omega)}{R_\pi^{\text{LO}}(0)}, \quad (69)$$

$$K_\sigma^{\text{LO}}(\omega) = -2J_\sigma^{\text{LO}}(\omega), \quad K_\sigma^{\text{NLO}}(\omega) = -2J_\sigma^{\text{NLO}}(\omega) - \frac{10}{9} \frac{R_{\sigma 2}^{\text{NLO}}(\omega)}{R_\pi^{\text{LO}}(0)},$$

where

$$R_{\sigma 1}^{\text{NLO}}(\omega) = -\frac{4m^2}{\omega^2} \int_0^\infty dt \tilde{\Phi}(m^2 t) \left\{ \frac{t}{1+t} [1 + D(t, \omega)] - \frac{3-\omega^2}{\omega^2} \text{Ln}_+(t, \omega) - \frac{1+2t}{(1+t)\omega} \text{Ln}_-(t, \omega) \right\}, \quad (70)$$

$$R_{\sigma 2}^{\text{NLO}}(\omega) = \frac{8m^2}{(1-\omega^2)} \int_0^\infty dt \tilde{\Phi}(m^2 t) \left\{ \frac{t}{t+1} - \frac{2-\omega^2}{\omega^2} \text{Ln}_+(t, \omega) - \frac{1}{\omega} \text{Ln}_-(t, \omega) \right\}.$$

Final numerical values for the expansion coefficients are:

$$\begin{aligned}
J_\sigma^{\text{LO}}(1) &= -\frac{K_\sigma^{\text{LO}}(1)}{2} = 0.54, & J_\sigma^{\text{LO}}(0) &= -\frac{K_\sigma^{\text{LO}}(0)}{2} = 0.23, \\
J_\sigma^{\text{NLO}}(1) &= 1.18 \text{ GeV}^2, & J_\sigma^{\text{NLO}}(0) &= 0.87 \text{ GeV}^2, \\
K_\sigma^{\text{NLO}}(1) &= 4.61 \text{ GeV}^2, & K_\sigma^{\text{NLO}}(0) &= -0.09 \text{ GeV}^2.
\end{aligned} \tag{71}$$

#### IV. THE SIGMA MESON IN STRONG AND WEAK DECAYS

In this section we derive the matrix elements describing the strong decay  $\sigma \rightarrow \pi\pi$  and the nonleptonic decays  $D \rightarrow \sigma\pi$  and  $B \rightarrow \sigma\pi$ .

##### A. Strong decay $\sigma \rightarrow \pi\pi$

The strong form factor  $G_{\sigma\pi\pi}(p^2, q_1^2, q_2^2)$  related to the transition  $\sigma \rightarrow \pi\pi$  is defined in our approach as

$$\begin{aligned}
G_{\sigma\pi\pi}(p^2, q_1^2, q_2^2) &= \frac{3g^3}{2\pi^2\sqrt{2}} \int \frac{d^4k}{4\pi^2i} \tilde{\Phi}(-k^2) \tilde{\Phi}\left(-\left[k + \frac{p_2}{2}\right]^2\right) \tilde{\Phi}\left(-\left[k - \frac{p_1}{2}\right]^2\right) \\
&\quad \times \text{tr}\left\{\gamma^5 S\left(k + \frac{p}{2}\right) S\left(k - \frac{p}{2}\right) \gamma^5 S\left(k + \frac{q}{2}\right)\right\}
\end{aligned} \tag{72}$$

The  $\sigma$  momentum is given by  $p$ , pion momenta are labeled by  $q_1$  and  $q_2$  with  $p = q_1 + q_2$  and  $q = q_2 - q_1$ . The matrix element of Eq. (72) was already introduced in its generic form by Eq. (18), when we discussed the model features. The corresponding evaluation is summarized in Appendix A.

Since the strong modes  $\sigma \rightarrow \pi^+\pi^-$  and  $\sigma \rightarrow \pi^0\pi^0$  dominate the  $\sigma$  decays, the total width  $\Gamma_\sigma$  is given by

$$\Gamma_\sigma \simeq \Gamma(\sigma \rightarrow \pi^+\pi^-) + \Gamma(\sigma \rightarrow \pi^0\pi^0). \tag{73}$$

With the coupling constant  $g_{\sigma\pi\pi} \doteq G_{\sigma\pi\pi}(M_\sigma^2, M_\pi^2, M_\pi^2)$  the total decay width  $\Gamma_\sigma$  can then be expressed as

$$\Gamma_\sigma = \frac{3}{2} \Gamma(\sigma \rightarrow \pi^+\pi^-) = \frac{3g_{\sigma\pi\pi}^2}{32\pi M_\sigma^3} \lambda^{1/2}(M_\sigma^2, M_\pi^2, M_\pi^2), \tag{74}$$

where  $\lambda^{1/2}(M_\sigma^2, M_\pi^2, M_\pi^2)$  was already defined in Eq. (40).

## B. Weak decays $D \rightarrow \sigma\pi$ and $B \rightarrow \sigma\pi$

Now we turn to the discussion of the nonleptonic two-body transitions  $H \rightarrow \sigma\pi$  with  $H = D$  or  $B$ . The corresponding decay width  $\Gamma(H \rightarrow \sigma\pi)$  is given by

$$\Gamma(H \rightarrow \sigma\pi) = \frac{g_{H\sigma\pi}^2}{16\pi M_H^3} \lambda^{1/2}(M_H^2, M_\sigma^2, M_\pi^2), \quad (75)$$

where  $g_{H\sigma\pi}$  is the effective weak coupling constant. The constant  $g_{H\sigma\pi}$  is equivalent to the expectation value of the effective Hamiltonian  $\mathcal{H}_{eff}$  as derived from the nonleptonic Lagrangian (15)

$$g_{H\sigma\pi} = \langle \sigma\pi | \mathcal{H}_{eff} | H \rangle = \frac{G_F}{\sqrt{2}} V_{cd}^* V_{ud} a_1^{F+NF;(Q)} F_0^{H\sigma}(M_\pi^2) (M_H^2 - M_\sigma^2) f_\pi, \quad (76)$$

where  $F_0^{H\sigma}$  is the weak form factor describing the  $H \rightarrow \sigma$  transition [14,15].

Following Refs. [15,17] we consider the two dominant (so-called "quark decay") graphs contributing to the form factor  $F_0^{H\sigma}$ : the direct (DR) diagram of Fig.6a and the resonance or polar (PR) diagram of Fig.6b with an intermediate axial meson  $H(1^+)$  (the charmed meson  $D(1^+)$  with a mass of  $M_{D(1^+)} = 2.422$  GeV [1] and the bottom meson  $B(1^+)$  with a mass of  $M_{B(1^+)} = 5.7$  GeV [17]). We neglect the suppressed "annihilation" diagram, that is the  $D \rightarrow W \rightarrow \sigma + \pi$  transition, since it involves form factors of light mesons at high momentum transfer ( $q^2 = M_D^2$ ) [28]. The individual contributions to the form factor  $F_0^{H\sigma}$  are given by

$$F_0^{H\sigma;DR}(q^2) = \frac{3g_H g_\sigma}{4\pi^2 \sqrt{2} (M_H^2 - M_\sigma^2)} I_{H\sigma}(q^2), \quad (77)$$

$$F_0^{H\sigma;PR}(q^2) = \frac{3g_H g_\sigma}{4\pi^2 \sqrt{2} (M_H^2 - M_\sigma^2)} \frac{3g_{H(1^+)}^2}{4\pi^2 M_{H(1^+)}^2} I_{HH(1^+)\sigma}(q^2) I_{H(1^+)}(q^2)$$

where  $I_{H\sigma}$ ,  $I_{HH(1^+)\sigma}^\mu$  and  $I_{H(1^+)}^\mu$  are the structure integrals:

$$I_{H\sigma}(q^2) = \int \frac{d^4 k}{4\pi^2 i} \tilde{\Phi}\left(-\left[k + \frac{p'}{2}\right]^2\right) \tilde{\Phi}_H(-(k + \omega_{Qq}p)^2) \times \text{tr} \left[ S_Q(\not{k} + \not{p}) \gamma^5 S(\not{k}) S(\not{k} + \not{p}') \not{q} \gamma^5 \right], \quad (78)$$

$$I_{HH(1^+)\sigma}(q^2) = \int \frac{d^4 k}{4\pi^2 i} \tilde{\Phi}\left(-\left[k + \frac{p'}{2}\right]^2\right) \tilde{\Phi}_H(-(k + \omega_{Qq}p)^2) \tilde{\Phi}_H(-(k + \omega_{Qq}p' + \omega_{Qq}p)^2) \times \text{tr} \left[ S_Q(\not{k} + \not{p}) \gamma^5 S(\not{k}) S(\not{k} + \not{p}') \not{q} \gamma^5 \right],$$

$$I_{H(1^+)}(q^2) = \frac{1}{q^2} \int \frac{d^4 k}{4\pi^2 i} \tilde{\Phi}_H(-(k + \omega_{Qq}q)^2) \text{tr} \left[ S_Q(\not{k} + \not{q}) \not{q} \gamma^5 S(\not{k}) \not{q} \gamma^5 \right],$$

with  $\omega_{Qq} = m_q/(m_Q + m_q)$ . Again, the analytical evaluation of the structure integrals, before the final numerical calculation is applied, is indicated in Appendix A.

## V. NUMERICAL ANALYSIS

### A. Electromagnetic form factors

Preliminary model results for the pion charge  $F_\pi(Q^2)$  and anomaly  $F_{\pi\gamma\gamma^*}(Q^2)$  form factors were already presented in Ref. [19]. Here we extend our formalism to the case of the  $\sigma\gamma\gamma$  form factors and we also perform a comprehensive analysis of the anomaly form factors.

Recently, new and more accurate experimental results for the charged pion electromagnetic form factor  $F_\pi(Q^2)$  were obtained by the Jefferson Lab  $F_\pi$  Collaboration [46]. These data for the momentum transfer region of  $Q^2 = 0.6 - 1.6$  GeV<sup>2</sup> were extracted from an analysis of electro-production of pions on the nucleon. The new results for the pion form factor lie somewhat higher than the older Cornell data points [47], but are consistent with a monopole parametrization fitted to elastic data at very low  $Q^2$  and with the  $1/Q^2$  scaling law [48]. In Fig.7 we show our results for  $F_\pi(Q^2)$  in the region up to  $Q^2 = 4$  GeV<sup>2</sup>. For comparison we indicate the experimental data, recent results ( $F_\pi$  Collaboration [46]) and previous ones (DESY [49] and CERN NA7 [50] Collaboration). We also indicate the predictions of other theoretical approaches: QCD sum rules [51], light-cone quark model [52], NJL model with a separable  $q\bar{q}$  interaction [53] and QCD modeling approach based on solutions of the Dyson-Schwinger equations [54]. Our model predictions provide a rather good description of the available data and are also close to the results of the QCD motivated approach [54], which is based on a similar physical picture. In contrast to the work of Ref. [54] we use, roughly speaking, simple phenomenological prescriptions for the quark propagator (a free propagator with an effective quark mass instead of a confined one) and for the meson correlation function. We also get a reasonable description of the pion charge radius with  $r_\pi = 0.65$  fm, as obtained in our model. Our result should be compared to the present world average data of  $r_\pi = (0.672 \pm 0.008)$  fm from PDG2002 [1], to the recent experimental result  $r_\pi = (0.65 \pm 0.05 \pm 0.06)$  fm of the SELEX Collaboration [55] and to the prediction of Ref. [54] with  $r_\pi = 0.67$  fm.

Next we discuss the numerical results for the  $\pi^0 \rightarrow \gamma\gamma$  transition form factor. First we consider our results for the form factor  $F_{\pi\gamma\gamma^*}(Q^2)$ , which are given in Fig. 8. The data points are taken from [56] (CELLO) and [40] (CLEO). Other theoretical calculations include the hard scattering approach (HSA) [57], QCD sum rules [58] and perturbative light-cone QCD [59]. Our curve for  $Q^2 F_{\gamma^*\gamma\pi}(Q^2)$  is in good agreement with the data and approaches the Brodsky-Lepage limit for large  $Q^2$ . With the usual definition for the range of a form factor, that is

$$\langle r_{H\gamma}^2 \rangle = -6 \frac{dF_{H\gamma\gamma^*}(Q^2)}{dQ^2} \Big|_{Q^2=0} \quad \text{with } H = \pi, \sigma, \quad (79)$$

we obtain for the radius of  $F_{\pi\gamma\gamma^*}(Q^2)$ :

$$\langle r_{\pi\gamma}^2 \rangle = 0.44 \text{ fm}^2. \quad (80)$$

Our result confirms the monopole-type approximation of the CLEO data [40] and is very close to the CELLO measurement [56] of  $\langle r_{\pi\gamma}^2 \rangle = 0.42 \pm 0.04$  fm<sup>2</sup>. Again, our model prediction is close to the result of a similar theoretical approach with  $\langle r_{\pi\gamma}^2 \rangle = 0.39 \pm 0.04$

fm<sup>2</sup> [45]. Fig.9 contains our results for the  $F_{\pi\gamma^*\gamma^*}(Q^2, \omega)$  form factor for different values of the asymmetry parameter  $\omega = 1, 3/4, 1/2$  and 0. An increase in  $\omega$  leads to a rise of  $F_{\pi\gamma^*\gamma^*}(Q^2, \omega)$  for large  $Q^2$ . Finally, for the anomaly coupling constant  $g_{\pi\gamma\gamma}$  and the decay width  $\Gamma_{\pi\gamma\gamma}$  our approach gives:

$$g_{\pi\gamma\gamma} = 0.263 \text{ GeV}^{-1} \quad \text{and} \quad \Gamma_{\pi\gamma\gamma} = 7.15 \text{ eV} \quad (81)$$

which is close to the data [1] of  $g_{\pi\gamma\gamma} = 0.273 \text{ GeV}^{-1}$  and  $\Gamma_{\pi\gamma\gamma} = 7.7 \pm 0.5 \pm 0.5 \text{ eV}$ .

Now we turn to the discussion of the  $Q^2$  dependence of  $F_{\sigma\gamma^*\gamma^*}$ . First we consider the limiting case  $\omega = 1$ , where one of the photons is virtual and the other one is real. The corresponding form factor  $F_{\sigma\gamma^*\gamma^*}(Q^2)$  is plotted in Fig.10. In the numerical calculation all three types of diagrams ( $\Delta$ , bubble and tadpole) are included. As was already stated before, the  $\Delta$  diagram gives the dominant contribution, whereas bubble and tadpole diagrams are significantly suppressed. Using Eq. (79) we determine the slope of the  $F_{\sigma\gamma^*\gamma^*}$  form factor as

$$\langle r_{\sigma\gamma}^2 \rangle = 0.40 \text{ fm}^2. \quad (82)$$

For completeness we also present the results for  $F_{\sigma\gamma^*\gamma^*}$  for different values of the asymmetry parameter  $\omega = 1, 3/4, 1/2$  and 0 in Fig. 11.

The coupling constant  $g_{\sigma\gamma\gamma}$  and, according to Eq. (35), the decay width  $\Gamma_{\sigma\gamma\gamma}$  are given in our approach as:

$$g_{\sigma\gamma\gamma} = 0.330 \text{ GeV}^{-1} \quad \text{and} \quad \Gamma_{\sigma\gamma\gamma} = 0.26 \text{ KeV}. \quad (83)$$

Again, the dominant contribution to  $g_{\sigma\gamma\gamma}$  arises from the triangle diagram. The separate contributions of the bubble (bub) and tadpole (tad) diagrams to the coupling constant are

$$g_{\sigma\gamma\gamma} \Big|_{\text{bub}} = -0.4 \times 10^{-4} \text{ GeV}^{-1} \quad \text{and} \quad g_{\sigma\gamma\gamma} \Big|_{\text{tad}} = -0.2 \times 10^{-4} \text{ GeV}^{-1}. \quad (84)$$

A variation of the  $\sigma$  meson mass in the region of  $0 \leq M_\sigma < 2m = 0.470 \text{ MeV}$  does not have much influence on the value for  $g_{\sigma\gamma\gamma}$  with  $g_{\sigma\gamma\gamma} \simeq 0.31 \pm 0.02 \text{ GeV}^{-1}$ . In the soft meson mass limit  $M_\pi^2 = M_\sigma^2 = 0$  we approximately reproduce the low-energy theorem:

$$g_{\pi\gamma\gamma} = \frac{9}{10} g_{\sigma\gamma\gamma} \simeq \frac{1}{4\pi^2 F_\pi}. \quad (85)$$

The anomaly constants calculated for zero meson mass values,  $g_{\pi\gamma\gamma} = 0.263 \text{ GeV}^{-1}$  and  $g_{\sigma\gamma\gamma} = 0.292 \text{ GeV}^{-1}$ , are rather close to the quantities predicted at  $M_\pi = 134.98 \text{ MeV}$  and  $M_\sigma = 385.4 \text{ MeV}$ .

Taking the recent result for the two-photon decay width of  $\sigma$  or  $f_0(400 - 1200)$  of  $\Gamma(f_0(400 - 1200) \rightarrow \gamma\gamma) = 3.8 \pm 1.5 \text{ KeV}$  [1,60] at face value, our direct result of Eq. (83) is off by about an order of magnitude. However, predictions for the decay width depend rather sensitively, that is to the third power, on the value of the scalar meson mass as evident from Eq. (35). Using our canonical value of  $g_{\sigma\gamma\gamma} = 0.330 \text{ GeV}^{-1}$ , which, as discussed, is fairly independent of the mass value, and varying the  $\sigma$  mass we obtain:

$M_\sigma, \text{ GeV}$		0.4		0.5		0.6		0.7		0.8		0.9		1		1.1		1.2		(86)
$\Gamma(\sigma \rightarrow \gamma\gamma), \text{ KeV}$		0.3		0.6		1		1.6		2.3		3.3		4.6		6.1		7.9		

The range of prediction can be summarized as  $\Gamma(\sigma \rightarrow \gamma\gamma) = 4.1 \pm 3.8 \text{ KeV}$ , which now is in qualitative agreement with the experimental result.

## B. Strong and weak decays

In the following we indicate the model predictions for strong and weak decay observables of the  $\sigma$  meson. Based on the definition given in Sec. IV A, our numerical result for the coupling constant of the strong decay  $\sigma \rightarrow \pi\pi$  is:

$$g_{\sigma\pi\pi} = 1.8 \text{ GeV}. \quad (87)$$

The value we obtain is close to the one extracted from the BES experiment [16] with  $g_{\sigma\pi\pi} = 2.0_{-0.19}^{+0.30}$  GeV and to the prediction of the linear  $\sigma$  model:

$$g_{\sigma\pi\pi} = \frac{M_\sigma^2}{F_\pi} = 1.6 \text{ GeV}. \quad (88)$$

In Eq. (88) we used the values  $M_\sigma = 385.4$  MeV and  $F_\pi = 92.7$  MeV as determined in our approach. Using Eq. (74) for the decay width of the  $\sigma$  meson we get  $\Gamma_\sigma = 173$  MeV. This value is smaller than the ones reported by the E791 ( $324_{-40}^{+42} \pm 21$  MeV) and the BES ( $282_{-50}^{+77}$  MeV) Collaborations. Again, a variation of the  $\sigma$  meson mass in the region  $0 \leq M_\sigma < 2m$  leads to a range of predictions for  $g_{\sigma\pi\pi}(M_\sigma^2) = 1.96 \pm 0.73$ . The central value of  $g_{\sigma\pi\pi}(M_\sigma^2)$  corresponds to  $M_\sigma \sim 350$  MeV, the upper limit to  $M_\sigma = 0$ , whereas the minimal value is obtained for a mass value near  $M_\sigma \sim 2m$ . Substituting the results for  $g_{\sigma\pi\pi}(M_\sigma^2)$  as a function  $M_\sigma$  into Eq.(74) we estimate the variation of the  $\sigma$  meson width as  $\Gamma_\sigma = 0 \div 206$  MeV. The lower limit corresponds obviously to the threshold  $M_\sigma = 2M_\pi$  and the largest value to  $M_\sigma \approx 330$  MeV.

Finally we discuss the results for the nonleptonic decays  $D \rightarrow \sigma\pi$  and  $B \rightarrow \sigma\pi$ . We first give our predictions for the weak form factors  $F_0^{D\sigma}(M_\pi^2)$  and  $F_0^{B\sigma}(M_\pi^2)$  of Eq. (77) evaluated at the physical point  $q^2 = M_p i^2$ :

$$F_0^{D\sigma}(M_\pi^2) = F_0^{D\sigma;\text{DR}}(M_\pi^2) + F_0^{D\sigma;\text{PR}}(M_\pi^2) = 0.368, \quad (89)$$

$$F_0^{D\sigma;\text{DR}}(M_\pi^2) = 0.298, \quad F_0^{D\sigma;\text{PR}}(M_\pi^2) = 0.070,$$

and

$$F_0^{B\sigma}(M_\pi^2) = F_0^{B\sigma;\text{DR}}(M_\pi^2) + F_0^{B\sigma;\text{PR}}(M_\pi^2) = 0.144, \quad (90)$$

$$F_0^{B\sigma;\text{DR}}(M_\pi^2) = 0.141, \quad F_0^{B\sigma;\text{PR}}(M_\pi^2) = 0.003.$$

With our results for  $F_0^{D\sigma}(M_\pi^2)$  and  $F_0^{B\sigma}(M_\pi^2)$  we get for the effective weak coupling constants (Eq. (76))

$$g_{D\sigma\pi} = 368 \text{ eV} \quad \text{and} \quad g_{B\sigma\pi} = 16.2 \text{ eV} \quad (91)$$

and finally for the decay widths, originally defined in Eq. (75),

$$\Gamma(D^+ \rightarrow \sigma\pi^+) = 1.37 \times 10^{-12} \text{ MeV} \quad \text{and} \quad \Gamma(B^+ \rightarrow \sigma\pi^+) = 0.98 \times 10^{-16} \text{ MeV}. \quad (92)$$

Our prediction for the decay width  $\Gamma(D \rightarrow \sigma\pi)$  is in good agreement with the central value of the E791 result [1,12] of:

$$\Gamma(D^+ \rightarrow \sigma\pi^+) = (1.32 \pm 0.31) \times 10^{-12} \text{ MeV} . \quad (93)$$

In our derivation we use a specific value for  $a_1^{\text{F+NF};(c)} = 1.274$  [29], a quantity which by Eq. (17) is related to a combination of Wilson coefficients occurring in the effective weak Lagrangian. Alternatively, if we use  $a_1^{\text{F+NF};(c)} = 1.1$  [28], which is fitted in a phenomenological analysis of nonleptonic D-decays under the factorization assumption, the result for the D decay is modified to

$$\Gamma(D^+ \rightarrow \sigma\pi^+) = 1.03 \times 10^{-12} \text{ MeV} \quad (94)$$

which is close to the lower limit of the experimental value.

We also compare our results to previous theoretical calculations done in Refs. [14,15,17]. A value for  $F_0^{D\sigma}(M_\pi^2)$  was estimated in Ref. [14] using the  $D \rightarrow \sigma\pi \rightarrow 3\pi$  data [12] without properly taking into account the rescattering effects. The result is  $F_0^{D\sigma}(M_\pi^2) = 0.79 \pm 0.15$ , which is twice as large as our prediction and also results in a value for the width  $\Gamma(D^+ \rightarrow \sigma\pi^+)$  larger than the measured one. Obviously, the value for  $F_0^{D\sigma}(M_\pi^2)$  should be directly extracted from the two-body transition  $D \rightarrow \sigma\pi$ .

In Ref. [15] the form factor  $F_0^{D\sigma}(M_\pi^2)$  was calculated (including direct and polar contributions) in a quark model similar to ours. The contribution of the direct diagram

$$F_0^{D\sigma;\text{DR}}(0) = 0.30 \pm 0.02 \quad (95)$$

is close to our result but the contribution of the polar diagram

$$F_0^{D\sigma;\text{PR}}(0) = 0.22_{-0.01}^{+0.07} \quad (96)$$

is larger. In total they get  $F_0^{D\sigma}(0) = 0.52_{-0.03}^{+0.09}$ , which when extrapolated to the point  $q^2 = M_\pi^2$  results in  $F_0^{D\sigma}(M_\pi^2) = 0.57 \pm 0.09$ . With the final result of  $\Gamma(D^+ \rightarrow \sigma\pi^+) = 2.3 \times 10^{-12} \text{ MeV}$  this approach overestimates the experimental result. This work was extended in Ref. [17] to determine the form factor  $F_0^{B\sigma}(M_\pi^2)$ . The result they obtain is

$$F_0^{B\sigma}(M_\pi^2) \simeq 0.45 \pm 0.15 . \quad (97)$$

which, again, is about three times larger than our prediction.

## VI. SUMMARY

In summary, we have applied the relativistic constituent quark model to investigate electromagnetic  $\pi$  and  $\sigma$  meson form factors and a variety of strong and weak decay characteristics involving the  $\sigma$ . We start with an effective quark-meson interaction Lagrangian, which is based on a linear realization of chiral symmetry. Then we write down the matrix elements describing the meson interactions in terms of a set of quark diagrams. All model parameters were previously determined [19]- [21] in a fit to experimental observables.

In a first step we present a detailed analysis of the electromagnetic form factors of the  $\pi$  and  $\sigma$  mesons. To solidify our model considerations, we study the electromagnetic form factor of the charged pion, which was recently measured by the Jefferson Lab  $F_\pi$  Collaboration [46]. We also calculate the form factors which govern the anomaly transitions  $H \rightarrow \gamma\gamma$  with  $H = \pi^0$  and  $\sigma$  including different kinematics of the photons. Our results for the pion are in good agreement with the recent experimental data [46,40]. We furthermore give results (analytical formulas and numerics) for the asymptotics of the anomaly form factors at large values of space-like photon virtualities. The behavior of the  $\pi^0\gamma\gamma^*$  form factor nicely coincides with the prediction of perturbative QCD [39]. Expressions for the leading order (LO)  $\sim 1/Q^2$  and the next-to-leading (NLO) order  $\sim 1/Q^4$  expansion coefficients in the form factors are calculated at arbitrary values of large photon virtualities. We complete the analysis by indicating results for the charge radii.

Based on the chiral symmetry construction we determine the  $\sigma$  meson mass  $M_\sigma = 385.4$  MeV and the total width  $\Gamma_\sigma = 173$  MeV. Both values are lower than the experimental values of the E791 [12] Collaboration, but close to the BES [13] results. The predicted strong coupling constant  $g_{\sigma\pi\pi} = 1.8$  GeV is fairly stable with respect to variations in the  $\sigma$  mass, but the total width, due to phase space, depends sensitively on this value. Turning to the experimental evidence for the  $\sigma$  meson we give predictions for the decay characteristics in the nonleptonic  $D \rightarrow \sigma\pi$  and  $B \rightarrow \sigma\pi$  transitions. Both form factors and decays widths are determined. Our result for  $\Gamma(D^+ \rightarrow \sigma\pi^+)$  is in very good agreement with the data [1,12] for both limiting cases: when we apply the factorization hypothesis we get  $\Gamma(D^+ \rightarrow \sigma\pi^+) = 1.03 \times 10^{-12}$  MeV and when we include nonfactorizable effects the result is changed to  $\Gamma(D^+ \rightarrow \sigma\pi^+) = 1.37 \times 10^{-12}$  MeV. Our prediction for the decay width  $\Gamma(B^+ \rightarrow \sigma\pi^+)$  is  $\Gamma(B^+ \rightarrow \sigma\pi^+) = 0.98 \times 10^{-16}$  MeV, which is expected to be measured in forthcoming experiments.

## Acknowledgments

A.F., Th.G. and V.E.L. thank the DFG grants FA67/25-1 and GRK683 for support. M.A.I. appreciates the partial support by the DFG grants GRK683 and 436 RUS17/47/02, the Russian Fund of Basic Research grant No. 01-02-17200 and the Heisenberg-Landau Program. P.W. thanks the Alexander von Humboldt Foundation for financial support.

## REFERENCES

- [1] K. Hagiwara *et al.*, Phys. Rev. D **66**, 010001 (2002).
- [2] N. A. Tornqvist, hep-ph/0008135; F. E. Close, N. A. Tornqvist, J. Phys. G **28**, R249 (2002).
- [3] J. Schwinger, Ann. Phys. (N.Y.) **2**, 407 (1957).
- [4] M. Gell-Mann and M. Levy, Nuovo. Cim. **122**, 705 (1960).
- [5] Y. Nambu and G. Jona-Lasinio, Phys. Rev. **122**, 345 (1961); **124**, 246 (1961).
- [6] J. Schechter and Y. Ueda, Phys. Rev. D **3**, 168 (1971).
- [7] S. Weinberg, Phys. Rev. Lett. **18**, 188 (1967); Phys. Rev. **166**, 1568 (1968).
- [8] S. Weinberg, Physica A **96** (1979) 327; J. Gasser and H. Leutwyler, Ann. Phys. (N.Y.) **158**, 142 (1984); Nucl. Phys. B **250**, 465 (1985).
- [9] G. Colangelo, J. Gasser and H. Leutwyler, Nucl. Phys. B **603**, 125 (2001).
- [10] J. Oller, E. Oset and J. R. Pelaez, Phys. Rev. Lett. **80** (1998) 3452.
- [11] F. Kleefeld, E. van Beveren, G. Rupp and M. D. Scadron, Phys. Rev. D **66**, 034007 (2002).
- [12] E791 Collaboration, E. M. Aitala *et al.*, Phys. Rev. Lett. **86**, 770 (2001).
- [13] N. Wu, hep-ex/0104050.
- [14] C. Dib and R. Rosenfeld, Phys. Rev. D **63**, 117501 (2001).
- [15] R. Gatto, G. Nardulli, A. D. Polosa and N. A. Törnqvist, Phys. Lett. B **494**, 168 (2000).
- [16] W. Huo, X. Zhang and T. Huang, Phys. Rev. D **65**, 097505 (2002).
- [17] A. Deandrea and A. D. Polosa, Phys. Rev. Lett. **86**, 216 (2001).
- [18] S. Gardner and Ulf-G. Meissner, Phys. Rev. D **65**, 094004 (2001).
- [19] M. A. Ivanov, M. P. Locher and V. E. Lyubovitskij, Few-Body Syst. **21**, 131 (1996); M. A. Ivanov and V. E. Lyubovitskij, Phys. Lett. B **408**, 435 (1997); I. V. Anikin, M. A. Ivanov, N. B. Kulimanova and V. E. Lyubovitskij, Z. Phys. C **65**, 681 (1995).
- [20] M. A. Ivanov, V. E. Lyubovitskij, J. G. Körner and P. Kroll, Phys. Rev. D **56**, 348 (1997); M. A. Ivanov, J. G. Körner, V. E. Lyubovitskij and A. G. Rusetsky, Phys. Rev. D **57**, 5632 (1998); D **60**, 094002 (1999); Phys. Lett. B **476**, 58 (2000); M. A. Ivanov and P. Santorelli, Phys. Lett. B **456**, 248 (1999); A. Faessler, T. Gutsche, M. A. Ivanov, J. G. Korner and V. E. Lyubovitskij, Phys. Lett. B **518**, 55 (2001).
- [21] A. Faessler, T. Gutsche, M. A. Ivanov, J. G. Korner and V. E. Lyubovitskij, Eur. Phys. J. direct **C4**, 18 (2002).
- [22] A. Salam, Nuovo Cim. **25**, 224 (1962); S. Weinberg, Phys. Rev. **130**, 776 (1963); K. Hayashi *et al.*, Fort. der Phys. **15**, 625 (1967).
- [23] G. V. Efimov and M. A. Ivanov, "The Quark Confinement Model of Hadrons", IOP Publishing, Bristol & Philadelphia, 1993.
- [24] T. Becher and H. Leutwyler, Eur. Phys. J. C **9**, 643 (1999); JHEP **0106**, 017 (2001).
- [25] G. Buchalla, A. J. Buras and M. E. Lautenbacher, Rev. Mod. Phys. **68**, 1125 (1996).
- [26] S. Mandelstam, Ann. Phys. (N.Y.) **19**, 1 (1962).
- [27] J. Terning, Phys. Rev. D **44**, 887 (1991).
- [28] M. Bauer, B. Stech and M. Wirbel, Z. Phys. C **34**, 103 (1987).
- [29] Hai-Yang Cheng, Eur. Phys. J. C **26**, 551 (2003).
- [30] M. Beneke, G. Buchalla, M. Neubert and C. T. Sachrajda, Phys. Rev. Lett. **83**, 1914 (1999).

- [31] S. Ryan: Nucl. Phys. B (Proc. Suppl.) **106**, 86 (2002).
- [32] S. Adler, Phys. Rev. **177** (1969) 2426;  
J. Bell and R. Jackiw, Nuovo Cimento A **60** (1969) 47.
- [33] M. Veltman, Proc. Roy. Soc. A **301**, 107 (1967); D. G. Sutherland, Nucl. Phys. B **2**, 433 (1967).
- [34] G. 't Hooft and M. Veltman, Nucl. Phys. B **44**, 189 (1972).
- [35] W. Pauli and F. Villars, Rev. Mod. Phys. B **21**, 434 (1949).
- [36] S. N. Gupta, Proc. Phys. Soc. A **66**, 129 (1953).
- [37] F. J. Yndurain, "Quantum Chromodynamics", Springer-Verlag Publishing, New-York, Berlin, Heidelberg & Tokyo, 1986.
- [38] G. 't Hooft and M.J.G. Veltman, Nucl. Phys. B **153**, 365 (1979).
- [39] S. J. Brodsky and G. P. Lepage, Phys. Rev. D **24**, 1808 (1981).
- [40] CLEO Collaboration, J. Gronberg *et al.*, Phys. Rev. D **57**, 33 (1998).
- [41] A. P. Bakulev, S. V. Mikhailov and N. G. Stefanis, hep-ph/0212250.
- [42] A. R. Zhitnitskij, I. R. Zhitnitskij and V. L. Chernyak, Sov. J. Nucl. Phys. **38**, 645 (1983).
- [43] V. A. Novikov, M. A. Shifman, A. I. Vainstein, M. B. Voloshin and V. I. Zakharov, Nucl. Phys. B **237**, 525 (1984).
- [44] G. Baur, K. Hencken, D. Trautman, S. Sadovsky and Yu. Kharlov, Phys. Rep. **364**, 359 (2002).
- [45] P. Maris and P. C. Tandy, Phys. Rev. C **65**, 045211 (2002).
- [46] The Jefferson  $F_\pi$  Collaboration, E. Volner *et al.*, Phys. Rev. Lett. **86**, 1713 (2001).
- [47] C. J. Bebek, Phys. Rev. D **17**, 1693 (1978).
- [48] V. A. Matveev, R. M. Muradyan and A. N. Tavkhelidze, Lett. Nuovo Cim. **7**, 719 (1973); S. J. Brodsky and G. R. Farrar, Phys. Rev. Lett. **31**, 1153 (1973).
- [49] P. Brauel *et al.*, Z. Phys. C **3**, 101 (1979).
- [50] CERN NA7 Collaboration, S. R. Amendolia *et al.*, Nucl. Phys. B **277**, 168 (1986).
- [51] V. A. Nesterenko and A. V. Radyushkin, Phys. Lett. B **115**, 410 (1982).
- [52] F. Cardarelli, E. Pace, G. Salme and S. Simula, Phys. Lett. B **357**, 267 (1995).
- [53] H. Ito, W. W. Buck and F. Gross, Phys. Rev. C **45**, 1918 (1992).
- [54] P. Maris and P. C. Tandy, Phys. Rev. C **62**, 055204 (2000).
- [55] SELEX Collaboration, I. Eschrich *et al.*, Phys. Lett. B **522**, 233 (2001).
- [56] CELLO Collaboration, H.-J. Behrend *et al.*, Z. Phys. C **49**, 401 (1991).
- [57] R. Jakob, P. Kroll and M. Raulfs, J. Phys. G **22**, 45 (1996).
- [58] A. V. Radyushkin and R. Ruskov, Nucl. Phys. B **481**, 625 (1996).
- [59] F.-G. Cao, T. Huang and B.-Q. Ma, Phys. Rev. D **53**, 6582 (1996).
- [60] M. Boglione and M. R. Pennington, Eur. Phys. J. C **9**, 11 (1999).

## APPENDIX

### A. Methods of calculation for matrix elements

We demonstrate the evaluation of matrix elements for the example of the derivative of the meson mass operator (4):

$$\tilde{\Pi}'_H(p^2) = -\frac{p^\alpha}{2p^2} \frac{d}{dp^\alpha} \int \frac{d^4k}{4\pi^2 i} \tilde{\Phi}_H^2(-k^2) \text{tr} \left[ \Gamma_H S_1(\not{k} + w_{21} \not{p}) \Gamma_H S_2(\not{k} - w_{12} \not{p}) \right]. \quad (98)$$

The technique we use is based on the three main ingredients:

- use of the Laplace transform of the vertex function

$$\tilde{\Phi}(z) = \int_0^\infty ds \Phi_L(s) e^{-sz},$$

- the  $\alpha$ -transform of the denominator

$$\frac{1}{m^2 - (k+p)^2} = \int_0^\infty d\alpha e^{-\alpha(m^2 - (k+p)^2)},$$

- and the differential representation of the numerator

$$(m + \not{k} + \not{p}) e^{kq} = \left( m + \gamma^\mu \frac{\partial}{\partial q^\mu} + \not{p} \right) e^{kq}.$$

After straightforward algebra we get expressions for the coupling constants  $h_H = 1/\tilde{\Pi}'_H(m_H^2)$  of pseudoscalar ( $H = P$ ) and scalar ( $H = S$ ) mesons, which are given by

$$\begin{aligned} h_H^{-1} &= \frac{1}{4} \int_0^\infty \frac{dt}{A^3} \int_0^1 d\alpha \left\{ -[\tilde{\Phi}^2(z_0)]' B \left( d_H \frac{m_1 m_2}{\Lambda_H^2} + \frac{m_H^2}{\Lambda_H^2} \frac{A(1 - \Delta^2) + B}{4A^2} \right) \right. \\ &\quad \left. + \tilde{\Phi}^2(z_0) \left( 1 - \Delta^2 + \frac{3B}{A} \right) \right\}, \end{aligned} \quad (99)$$

where  $[\tilde{\Phi}^2(z_0)]' = d[\tilde{\Phi}^2(z_0)]/dz_0$ ,  $d_H = 1$  for pseudoscalar mesons and  $d_H = -1$  for scalar mesons. We also define

$$z_0 = \frac{B}{4} [(m_1 + m_2)^2 - m_H^2] + \frac{m_H^2 t^2}{4A} (2\alpha - 1 + \Delta)^2,$$

$$A = 1 + t, \quad B = t[4\alpha(1 - \alpha)A + (2\alpha - 1 + \Delta)^2], \quad \Delta = w_{21} - w_{12}.$$

In analogy we consider the basic vertex function (18):

$$\Lambda^{12;13;23}(p_1, p_2) = \frac{3}{4\pi^2} g_{H_{13}} g_{H_{23}} g_{H_{12}} I^{12;13;23}(p_1, p_2) \quad (100)$$

$$I^{12;13;23}(p_1, p_2) = - \int \frac{d^4 k}{4\pi^2 i} \tilde{\Phi}_{H_{13}}(-(k + w_{13} p_1)^2) \tilde{\Phi}_{H_{23}}(-(k + w_{23} p_2)^2) \\ \times \tilde{\Phi}_{H_{12}}(-(k + w_{12} p_1 + w_{21} p_2)^2) \text{tr}[S_2(\not{k} + \not{p}_2) \Gamma_{H_{12}} S_1(\not{k} + \not{p}_1) \Gamma_{H_{13}} S_3(\not{k}) \Gamma_{H_{23}}]$$

Here we indicate the resulting expression for the Gaussian meson-quark vertex function  $\tilde{\Phi}_H(k_E^2) = \exp(-k_E^2/\Lambda_H^2)$ :

$$I^{12;13;23}(p_1, p_2) = \int_0^\infty \frac{dt t}{A^2} \int_0^1 d^3 \alpha \delta\left(1 - \sum_{i=1}^3 \alpha_i\right) \exp\left(-\frac{z}{\Lambda_{\text{red}}^2}\right) \left(\frac{C_1}{\Lambda_{\text{red}}^2} - \frac{C_2}{2A}\right), \quad (101)$$

where

$$C_1 = \frac{1}{4} \text{tr}[(m_2 + \not{D}_2) \Gamma_{12} (m_1 + \not{D}_1) \Gamma_{13} (m_3 + \not{D}_3) \Gamma_{23}],$$

$$C_2 = \frac{1}{4} \text{tr}[\gamma^\sigma \Gamma_{12} \gamma_\sigma \Gamma_{13} (m_3 + \not{D}_3) \Gamma_{23} + \gamma^\sigma \Gamma_{12} (m_1 + \not{D}_1) \Gamma_{13} \gamma_\sigma \Gamma_{23} + (m_2 + \not{D}_2) \Gamma_{12} \gamma^\sigma \Gamma_{13} \gamma_\sigma \Gamma_{23}],$$

$$D_1 = p_1 - p_t, \quad D_2 = p_2 - p_t, \quad D_3 = -p_t, \quad p_t = r_1 p_1 + r_2 p_2,$$

$$r_1 = \frac{1}{A} (t\alpha_1 + w_{13}s_{13} + w_{12}s_{12}), \quad r_2 = \frac{1}{A} (t\alpha_2 + w_{23}s_{23} + w_{12}s_{21}),$$

$$z = t \left[ \sum_{i=1}^3 \alpha_i m_i^2 - \alpha_1 p_1^2 - \alpha_2 p_2^2 \right] + A \left[ (r_1 + r_2)(r_1 p_1^2 + r_2 p_2^2) - r_1 r_2 p_3^2 \right] \\ - p_1^2 (w_{13}^2 s_{13} + w_{12} s_{12}) - p_2^2 (w_{23}^2 s_{23} + w_{21} s_{12}) + p_3^2 w_{12} w_{21} s_{12},$$

$$\frac{1}{\Lambda_{\text{red}}^2} = \frac{1}{\Lambda_{H_{12}}^2} + \frac{1}{\Lambda_{H_{13}}^2} + \frac{1}{\Lambda_{H_{23}}^2}, \quad s_{ij} = \frac{\Lambda_{\text{red}}^2}{\Lambda_{ij}^2}.$$

All further calculations are done by using computer programs written in FORM for the manipulations of Dirac matrices and in FORTRAN for the final numerical evaluations.

## B. Feynman rules for nonlocal electromagnetic vertices

In the following we derive the Feynman rules for the nonlocal vertices of Figs.3a and 3b. These vertices contain the path integral over the gauge field  $I(x, y, P)$ . The crucial point is to calculate the expression

$$\tilde{\Phi}(\partial_x^2) e^{ipx} [I(x, y, P)]^N \quad (102)$$

using Eq.(14). The case  $N = 1$  corresponds to the vertex of Fig.3a and  $N = 2$  to the vertex of Fig.3b.

First, we consider the case  $N = 1$ . It is readily seen that

$$\tilde{\Phi}(\partial_x^2)e^{ipx}I(x, y, P) = e^{ipx}\tilde{\Phi}(\mathcal{D}_x^2)I(x, y, P) \quad (103)$$

where  $\mathcal{D}_x \equiv \partial_x + ip$ . Thus we have to calculate

$$\tilde{\Phi}(\mathcal{D}_x^2)I(x, y, P) = \sum_{n=0}^{\infty} \frac{\tilde{\Phi}^{(n)}(0)}{n!} \mathcal{D}_x^{2n} I(x, y, P). \quad (104)$$

One finds that

$$\mathcal{D}_x^2 I(x, y, P) = [\partial_x A(x) + 2ipA(x)] - p^2 I(x, y, P) \equiv L(A) - p^2 I(x, y, P) \quad (105)$$

where  $L(A) \equiv \partial_x A(x) + 2ipA(x)$ .

Iteration of the last expression

$$\begin{aligned} (\mathcal{D}_x^2)^2 I(x, y, P) &= (\mathcal{D}_x^2 - p^2)L(A) + (-p^2)^2 I(x, y, P) \\ (\mathcal{D}_x^2)^3 I(x, y, P) &= (\mathcal{D}_x^4 - \mathcal{D}_x^2 p^2 + p^4)L(A) + (-p^2)^3 I(x, y, P) \\ &\dots \\ (\mathcal{D}_x^2)^n I(x, y, P) &= \sum_{k=0}^{n-1} (\mathcal{D}_x^2)^{n-1-k} (-p^2)^k L(A) + (-p^2)^n I(x, y, P) \\ &= n \int_0^1 dt [\mathcal{D}_x^2 t - p^2(1-t)]^{n-1} L(A) + (-p^2)^n I(x, y, P) \end{aligned} \quad (106)$$

finally leads to

$$\begin{aligned} \tilde{\Phi}(\mathcal{D}_x^2)I(x, y, P) &= \int_0^1 dt \tilde{\Phi}'[\mathcal{D}_x^2 t - p^2(1-t)] L(A) + \tilde{\Phi}(-p^2) I(x, y, P) \\ &= \int \frac{d^4 q}{(2\pi)^4} A_\mu(q) \left\{ i(2p+q)^\mu e^{iqx} \int_0^1 dt \tilde{\Phi}'[-(p+q)^2 t - p^2(1-t)] \right. \\ &\quad \left. + \tilde{\Phi}(-p^2) \int_y^x dz^\mu e^{iqz} \right\} \end{aligned} \quad (107)$$

where  $A_\mu(q)$  is the Fourier-transform of the electromagnetic field and  $\tilde{\Phi}'(z) = d\tilde{\Phi}(z)/dz$ . The last term in Eq.(107) containing an integration from  $y$  to  $x$  (path integral) vanishes due to the delta function  $\delta(x-y)$  in the Lagrangian.

In complete analogy, we also obtain for the nonlocal vertex for the case  $N = 2$ :

$$\begin{aligned} \tilde{\Phi}(\mathcal{D}_x^2)I^2(x, y, P) &= \int \frac{d^4 q_1}{(2\pi)^4} \int \frac{d^4 q_2}{(2\pi)^4} A_\mu(q_1) A_\nu(q_2) \\ &\quad \times \left\{ 2g^{\mu\nu} e^{i(q_1+q_2)x} \int_0^1 dt \tilde{\Phi}'[-(p+q_1+q_2)^2 t - p^2(1-t)] \right. \\ &\quad \left. - (2p+q_1)^\mu (2p+2q_1+q_2)^\nu e^{i(q_1+q_2)x} \int_0^1 dt t \int_0^1 dl \right\} \end{aligned} \quad (108)$$

$$\begin{aligned}
& \times \tilde{\Phi}''[-l(t(p+q_1+q_2)^2 + p^2(1-t)) - (1-l)(t(p+q_1)^2 + (1-t)p^2)] \\
& - (2p+q_2)^\nu (2p+2q_2+q_1)^\mu e^{i(q_1+q_2)x} \int_0^1 dt t \int_0^1 dl \\
& \times \tilde{\Phi}''[-l(t(p+q_1+q_2)^2 + p^2(1-t)) - (1-l)(t(p+q_2)^2 + (1-t)p^2)] \\
& + i(2p+q_1)^\mu e^{iq_1x} \int_0^1 dt \tilde{\Phi}'[-(p+q_1)^2t - p^2(1-t)] \int_y^x dz^\mu e^{iq_2z} \\
& + i(2p+q_2)^\nu e^{iq_2x} \int_0^1 dt \tilde{\Phi}'[-(p+q_2)^2t - p^2(1-t)] \int_y^x dz^\mu e^{iq_1z} \\
& + g^{\mu\nu} \tilde{\Phi}(-p^2) \int_y^x dz^\mu e^{iq_1z} \int_y^x dw^\nu e^{iq_2w} \Big\} ,
\end{aligned}$$

where  $\tilde{\Phi}''(z) = d^2\tilde{\Phi}(z)/dz^2$ . Again, the last three terms in Eq.(108) containing integrations from  $y$  to  $x$  vanish due to the delta function.

### C. Form factors characterizing the local $\sigma \rightarrow \gamma\gamma$ diagram

In the following we give the full analytical expressions for the form factors of Eq. (44):

$$\begin{aligned}
F_L^\sigma = \frac{m}{\lambda^2} \Big\{ & -2(p^2 - q_1^2 - q_2^2)\lambda - 2L_1q_1^2(\lambda - 6q_2^2(q_2^2 - q_1^2 - p^2)) \\
& - 2L_2q_2^2(\lambda - 6q_1^2(q_1^2 - q_2^2 - p^2)) \\
& + 2L_3(q_1^6 + q_2^6 - q_1^4q_2^2 - q_1^2q_2^4 - 2q_1^4p^2 - 2q_2^4p^2 + q_1^2p^4 + q_2^2p^4 + 8q_1^2q_2^2p^2) \\
& + I_L(p^2, q_1^2, q_2^2)(p^2 - q_1^2 - q_2^2)(4m^2\lambda - p^6 + q_1^6 + q_2^6 - q_1^4q_2^2 - q_1^2q_2^4 \\
& - 3q_1^4p^2 - 3q_2^4p^2 + 3q_1^2p^4 + 3q_2^2p^4 + 10q_1^2q_2^2p^2) \Big\} ,
\end{aligned} \tag{109}$$

$$\begin{aligned}
G_L^\sigma = \frac{m}{\lambda^2} \Big\{ & 4\lambda + 4L_1(\lambda - 3q_1^2(q_1^2 + q_2^2 + p^2)) + 4L_2(\lambda - 3q_2^2(q_1^2 + q_2^2 + p^2)) \\
& + 4L_3(\lambda - 3p^2(q_1^2 + q_2^2 + p^2)) \\
& - 2I_L(p^2, q_1^2, q_2^2)(4m^2\lambda + p^6 + q_1^6 + q_2^6 - q_1^4q_2^2 - q_1^2q_2^4 - q_1^4p^2 - q_2^4p^2 \\
& - q_1^2p^4 - q_2^2p^4 + 6q_1^2q_2^2p^2) \Big\}
\end{aligned} \tag{110}$$

where  $I_L(p^2, q_1^2, q_2^2)$  is the integral defined in Eq. (38). Here we use

$$L_i = \int_0^1 dx \ln \left[ 1 - x(1-x) \frac{q_i^2}{m^2} \right] = -2 + 2 \sqrt{\frac{4m^2 - q_i^2}{q_i^2}} \text{ArcTan} \left( \sqrt{\frac{q_i^2}{4m^2 - q_i^2}} \right) \tag{111}$$

with  $q_3 \equiv p$ .

### D. Two-loop integral representation and power expansion of $I_{NL}$

The integral  $I_{NL}$  of Eq. (47), which is related to the  $\pi^0\gamma\gamma$  form factor, can be reduced to the two-loop integral

$$I_{\text{NL}} = - \int_0^\infty dt \frac{t}{1+t} \int_0^1 dx \left\{ \frac{\tilde{\Phi}(z_p)}{t A_1(x) + \Delta_1} - \frac{(1 - \alpha_0) \tilde{\Phi}(z_{q_2})}{t A_2(x) + \Delta_1} - \frac{\alpha_0 \tilde{\Phi}(z_{q_1})}{t A_3(x) + \Delta_1} \right\}, \quad (112)$$

where

$$\begin{aligned} z_p &= \frac{t^2}{1+t} D_p + \frac{t}{1+t} \Delta(1) & D_p &= m^2 - x(1-x)p^2 \\ z_{q_i} &= \frac{t^2}{1+t} D_{q_i} + \frac{t}{1+t} \Delta(x) & D_{q_i} &= m^2 - x(1-x)q_i^2 \\ \Delta(x) &= \Delta_0 + x \Delta_1 & \Delta_0 &= m^2 + p^2/4 - (q_1^2 + q_2^2)/2 \\ A_1(x) &= x \cdot \lambda^{1/2} + q_1^2 - \alpha_0 p^2 & \Delta_1 &= -p^2/2 + (q_1^2 + q_2^2)/2 \\ A_2(x) &= (1 - \alpha_0) x \cdot \lambda^{1/2} - (1 - \alpha_0) q_1^2 - \alpha_0 q_2^2 \\ A_3(x) &= -\alpha_0 x \cdot \lambda^{1/2} - (1 - \alpha_0) q_1^2 - \alpha_0 q_2^2 \end{aligned}$$

With the constraint that  $p^2 \leq 4m^2$  and  $q_i^2 \leq 0$  the variable  $t$  is replaced by  $u = t^2 D/(1+t) + t \Delta/(1+t)$  in the integral of Eq. (112):

$$\begin{aligned} I_{\text{NL}} &= \int_0^\infty du \tilde{\Phi}(u) \int_0^1 dx \left\{ - \frac{1}{R_p(1)} \frac{u - \Delta(1) + R_p(1)}{[u - \Delta(1) + R_p(1)] \cdot A_1(x) + 2 D_p \Delta_1} \right. \\ &\quad + \frac{1}{R_{q_2}(x)} \frac{(1 - \alpha_0) [u - \Delta(x) + R_{q_2}(x)]}{[u - \Delta(x) + R_{q_2}(x)] \cdot A_2(x) + 2 D_{q_2} \Delta_1} \\ &\quad \left. + \frac{1}{R_{q_1}(x)} \frac{\alpha_0 [u - \Delta(x) + R_{q_1}(x)]}{[u - \Delta(x) + R_{q_1}(x)] \cdot A_3(x) + 2 D_{q_1} \Delta_1} \right\}, \quad (113) \end{aligned}$$

where  $R_p(x) = \sqrt{(u - \Delta(x))^2 + 4u D_p}$ .

Next we perform a power expansion of  $I_{\text{NL}}$  in the limit  $p^2 = 0$ . For this kinematics we have

$$\begin{aligned} D &= m^2 + \frac{1}{2} \alpha_3 Q^2 (\alpha_1 (1 + \omega) + \alpha_2 (1 - \omega)), \\ \Delta &= m^2 + \frac{1}{2} \alpha_3 Q^2. \end{aligned} \quad (114)$$

By scaling the variable  $\alpha_3 \rightarrow \alpha_3/Q^2$  one finds

$$I_{\text{NL}} = - \frac{1}{Q^2} \int_0^\infty dt \left( \frac{t}{1+t} \right)^2 \int d^3 \alpha \delta \left( 1 - \alpha_1 - \alpha_2 - \frac{\alpha_3}{Q^2} \right) \tilde{\Phi}' \left( t m^2 + \frac{t \alpha_3 W}{2(1+t)} \right), \quad (115)$$

where

$$W = 1 + t [\alpha_1 (1 + \omega) + \alpha_2 (1 - \omega)]. \quad (116)$$

From the last expression it is easy to determine the asymptotics in the leading order (LO) with

$$(I_{\text{NL}})_{\text{LO}} = \frac{1}{Q^2} R_{\pi}^{\text{LO}}(\omega). \quad (117)$$

By using the formulas

$$\int d^2\alpha \delta(1 - \alpha_1 - \alpha_2) F(\alpha_1, \alpha_2) = \int d^2\alpha \delta(1 - \alpha_1 - \alpha_2) \left( F(0, 1) + F'_{\alpha_1}(\alpha_1, \alpha_2) \right), \quad (118)$$

$$\int_0^{\infty} dt g(t) \int_{tm^2}^{\infty} d\tau f(\tau) = m^2 \int_0^{\infty} dt f(tm^2) \int_0^t d\tau g(\tau),$$

where  $F'_{\alpha_1}(\alpha_1, \alpha_2) = \partial F(\alpha_1, \alpha_2)/\partial\alpha_1$ , the next-to-leading (NLO) term is obtained as

$$(I_{\text{NL}})_{\text{NLO}} = \frac{1}{Q^4} R_{\pi}^{\text{NLO}}(\omega). \quad (119)$$

Note that both integrals  $R_{\pi}^{\text{LO}}(\omega)$  and  $R_{\pi}^{\text{NLO}}(\omega)$  are defined in Eq. (52).

### E. Form factors characterizing the gauge-invariant part of the nonlocal triangle $\sigma \rightarrow \gamma\gamma$ diagram

Here we give the full analytical expressions for the form factors of Eqs. (62) and (63):

$$\begin{aligned} F_{\Delta_{\perp}}^{\sigma} = \frac{m}{\lambda^2} \bigg\{ & 8(S_q - S_p)(\lambda + 6q_1^2 q_2^2) + 2L_1^{\text{NL}} q_1^2 (\lambda - 12q_2^4 + 12q_2^2 p^2) \\ & + 2L_2^{\text{NL}} q_2^2 (\lambda - 12q_1^4 + 12q_1^2 p^2) \\ & - 2L_3^{\text{NL}} (q_1^6 + q_2^6 - q_1^4 q_2^2 - q_2^4 q_1^2 - 2q_1^4 p^2 - 2q_2^4 p^2 + q_1^2 p^4 + q_2^2 p^4 + 8q_1^2 q_2^2 p^2) \\ & + 6V_{11} q_1^2 (q_1^2 + q_2^2 - p^2)(q_1^2 + 3q_2^2 - p^2) - 6V_{12} q_1^2 (q_1^2 - q_2^2 - p^2)(q_1^2 + q_2^2 - p^2) \\ & + 6V_{21} q_2^2 (q_1^2 + q_2^2 - p^2)(3q_1^2 + q_2^2 - p^2) + 6V_{22} q_2^2 (q_1^2 + q_2^2 - p^2)(q_1^2 - q_2^2 + p^2) \\ & + I_{\text{NL}}(p^2, q_1^2, q_2^2) (p^2 - q_1^2 - q_2^2) (4m^2 \lambda - p^6 + q_1^6 + q_2^6 - q_1^4 q_2^2 - q_2^4 q_1^2 \\ & - 3q_1^4 p^2 - 3q_2^4 p^2 + 3q_1^2 p^4 + 3q_2^2 p^4 + 10q_1^2 q_2^2 p^2) \bigg\} \end{aligned} \quad (120)$$

$$\begin{aligned} G_{\Delta_{\perp}}^{\sigma} = \frac{m}{\lambda^2} \bigg\{ & \frac{2}{q_1^2 q_2^2} (S_q - S_p) (q_1^2 + q_2^2 - p^2)(\lambda + 12q_1^2 q_2^2) \\ & + 4L_1^{\text{NL}} (q_1^4 - 2q_2^4 - 2p^4 - 5q_1^2 q_2^2 + q_1^2 p^2 + 4q_2^2 p^2) \\ & - 4L_2^{\text{NL}} (2q_1^4 - q_2^4 + 2p^4 + 5q_1^2 q_2^2 - 4q_1^2 p^2 - q_2^2 p^2) \\ & - 4L_3^{\text{NL}} (q_1^4 + q_2^4 - 2p^4 - 2q_1^2 q_2^2 + q_1^2 p^2 + q_2^2 p^2) \\ & + 2V_{11} \frac{1}{q_2^2} (q_1^2 + 3q_2^2 - p^2)(\lambda + 6q_1^2 q_2^2) - 2V_{12} \frac{1}{q_2^2} (q_1^2 - q_2^2 - p^2)(\lambda + 6q_1^2 q_2^2) \\ & + 2V_{21} \frac{1}{q_1^2} (3q_1^2 + q_2^2 - p^2)(\lambda + 6q_1^2 q_2^2) + 2V_{22} \frac{1}{q_1^2} (q_1^2 - q_2^2 + p^2)(\lambda + 6q_1^2 q_2^2) \\ & - 2I_{\text{NL}}(p^2, q_1^2, q_2^2) (4m^2 \lambda + p^6 + q_1^6 + q_2^6 - q_1^4 q_2^2 - q_2^4 q_1^2 - q_1^4 p^2 - q_2^4 p^2 \\ & - q_1^2 p^4 - q_2^2 p^4 + 6q_1^2 q_2^2 p^2) \bigg\} \end{aligned} \quad (121)$$

where  $I_{\text{NL}}(p^2, q_1^2, q_2^2)$  is the three-dimensional integral of Eq. (47). Above we introduce the terms

$$S_r = \int_0^\infty dt \frac{t}{1+t} \left( m^2 - \frac{1}{(1+t)^2} \frac{r^2}{4} \right) \tilde{\Phi}(z_r), \quad (122)$$

$$L_i^{\text{NL}} = \int_0^\infty dt \frac{t}{(1+t)^2} \int_0^1 dx \tilde{\Phi}(z_i), \quad (123)$$

$$V_{i1} = \int_0^\infty dt \frac{t^2}{(1+t)^3} \int_0^1 dx x \tilde{\Phi}(z_i), \quad (124)$$

$$V_{i2} = \int_0^\infty dt \frac{t^2}{(1+t)^3} \int_0^1 dx (1-x) \tilde{\Phi}(z_i), \quad (125)$$

where

$$\begin{aligned} z_r &= m^2 t - \frac{r^2}{4} \frac{t}{1+t}, \quad (r = p, q), \\ z_i &= \frac{t^2}{1+t} (m^2 - x(1-x)q_i^2) + \frac{t}{1+t} \left( m^2 - \frac{p^2}{4} + \frac{x}{2}(p^2 - q_1^2 - q_2^2) \right), \quad (i = 1, 2), \\ z_3 &= \frac{t^2}{1+t} (m^2 - x(1-x)p^2) + \frac{t}{1+t} \left( m^2 - \frac{p^2}{4} \right). \end{aligned}$$

The asymptotics of these expressions can be derived from their representation in a manner as discussed for the  $\pi\gamma\gamma$  form factor in Appendix D. Here we obtain

$$\begin{aligned} (F_{\Delta_\perp}^\sigma)_{\text{LO}} &= -\frac{m}{Q^2 \omega^2} \left\{ R_\pi^{\text{LO}}(\omega) - \frac{2}{3} R_\pi^{\text{NLO}}(\omega) \right\}, \quad (126) \\ (F_{\Delta_\perp}^\sigma)_{\text{NLO}} &= -\frac{m^3}{Q^4} R_{\sigma 1}^{\text{NLO}}(\omega), \\ (G_{\Delta_\perp}^\sigma)_{\text{LO}} &= -\frac{2}{Q^2} (F_{\Delta_\perp}^\sigma)_{\text{LO}}, \\ (G_{\Delta_\perp}^\sigma)_{\text{NLO}} &= -\frac{2}{Q^2} (F_{\Delta_\perp}^\sigma)_{\text{NLO}} - \frac{8m}{Q^6} R_{\sigma 2}^{\text{NLO}}(\omega). \end{aligned}$$

The integrals  $R_{\sigma 1}^{\text{NLO}}(\omega)$  and  $R_{\sigma 2}^{\text{NLO}}(\omega)$  are defined in Eq. (70). The last simple relation between  $(F_{\Delta_\perp}^\sigma)_{\text{LO}}$  and  $(G_{\Delta_\perp}^\sigma)_{\text{LO}}$  is derived with the help of the identity

$$t\omega(\alpha_1 - \alpha_2) = W - (1 + t(\alpha_1 + \alpha_2)), \quad (127)$$

where  $W$  is defined in Eq. (116), and the exchange symmetry  $\alpha_1 \leftrightarrow \alpha_2$ .

## F. Form factors characterizing the gauge-invariant part of the nonlocal bubble and tadpole $\sigma\gamma\gamma$ diagrams

The gauge invariant parts of the nonlocal  $\sigma\gamma\gamma$  bubble (bub) diagram introduced in Eq. (60) are written as:

$$F_{\text{bub}_\perp}^\sigma = \frac{m}{2} \int_0^\infty dt \frac{t^2}{(1+t)^4} \int_0^1 d\tau \tau \int_0^1 dx (1-2x)(\tilde{\Phi}'(z_1) + \tilde{\Phi}'(z_2)), \quad (128)$$

$$G_{\text{bub}_\perp}^\sigma = -\frac{m}{q_1^2 q_2^2} \int_0^\infty dt \frac{t}{(1+t)^3} \int_0^1 d\tau \int_0^1 dx \left\{ \tilde{\Phi}(z_1) + \tilde{\Phi}(z_2) \right. \\ \left. + \frac{1}{4} (p^2 - q_1^2 - q_2^2) \frac{t\tau}{1+t} (1-2x)(\tilde{\Phi}'(z_1) + \tilde{\Phi}'(z_2)) \right\}, \quad (129)$$

where

$$z(q_1, q_2) = t \left( m^2 - x(1-x)q_1^2 \right) + \frac{t\tau}{1+t} (1-2x) \frac{p^2 - q_1^2 - q_2^2}{4} \\ - \frac{\tau(1-\tau+t)}{1+t} \frac{q_2^2}{4} - \frac{t}{1+t} (1-2x)^2 \frac{q_1^2}{4}, \\ z_1 = z(q_1, q_2), \quad z_2 = z(q_2, q_1).$$

The final expressions for the tadpole (tad) diagram, originally defined in Eq. (61), are

$$F_{\text{tad}_\perp}^\sigma = -\frac{m}{4} \int_0^\infty dt \frac{1}{(1+t)^3} \int_0^1 d\tau \tau^2 \int_0^1 dl l \\ \times \left\{ \tilde{\Phi}'(z_1) + \tilde{\Phi}'(z_2) - \tilde{\Phi}'(z_3) - \tilde{\Phi}'(z_4) \right\} \left( 1 - \frac{\tau}{1+t} \right), \quad (130)$$

$$G_{\text{tad}_\perp}^\sigma = \frac{m}{8q_1^2 q_2^2} \int_0^\infty dt \frac{1}{(1+t)^2} \int_0^1 d\tau \int_0^1 dl \left\{ 4(\tilde{\Phi}(z_p) + \tilde{\Phi}(z_q)) \right. \\ \left. + \frac{l\tau^2(1+t-\tau)}{(1+t)^2} (q_1^2 + q_2^2 - p^2) (\tilde{\Phi}'(z_1) + \tilde{\Phi}'(z_2) - \tilde{\Phi}'(z_3) - \tilde{\Phi}'(z_4)) \right. \\ \left. - \frac{4}{1+t} (\tilde{\Phi}(z_1) + \tilde{\Phi}(z_2) - \tilde{\Phi}(z_3) + \tilde{\Phi}(z_4)) \right\}, \quad (131)$$

where

$$z(p) = m^2 t - \frac{p^2}{4} \tau \frac{1+t-\tau}{1+t}, \quad z_p = z(p), \quad z_q = z(q), \quad z_i = m^2 t - W_i - R_i \frac{1+t-\tau}{1+t}, \\ W(q) = \frac{q^2}{4} \tau l (1-l), \quad R(q_1, q_2, l) = \frac{\tau^2}{4} \left( l[p^2 - q_1^2 - q_2^2] + l^2 q_1^2 + q_2^2 \right), \\ W_1 = W_3 = W(q_1), \quad W_2 = W_4 = W(q_2), \\ R_1 = R(q_1, q_2, l), \quad R_2 = R(q_2, q_1, l), \quad R_3 = R(q_1, q_2, -l), \quad R_4 = R(q_2, q_1, -l).$$

## TABLES

TABLE I. Leptonic decay constants  $f_P$  (MeV) used in the least-square fit. Data are either taken from PDG [1] or from the Lattice [31] (quenched (upper line) and unquenched (lower line)).

Meson	This model	Expt/Lattice
$\pi^+$	131	$130.7 \pm 0.1 \pm 0.36$
$K^+$	161	$159.8 \pm 1.4 \pm 0.44$
$D^+$	211	$203 \pm 14$
		$226 \pm 15$
$D_s^+$	222	$230 \pm 14$
		$250 \pm 30$
$B^+$	180	$173 \pm 23$
		$198 \pm 30$
$B_s^0$	196	$200 \pm 20$
		$230 \pm 30$
$B_c^+$	398	

## FIGURES

Fig.1: Meson mass operator.

Fig.2: Hadronic decay  $H_{13} \rightarrow H_{12} + H_{23}$ .

Fig.3: Nonlocal coupling of meson, quark and photon fields:  
one-photon vertex (3a), two-photon vertex (3b).

Fig.4: Diagrams contributing to the electromagnetic form factor  $F_\pi(Q^2)$  of the pion:  
triangle (4a) and bubble diagrams (4b and 4c).

Fig.5: Diagrams contributing to the anomaly processes  $H \rightarrow \gamma^*\gamma^*$ :  
triangle (5a), bubble (5b and 5c) and tadpole diagrams (5d).

Fig.6: Diagrams contributing to the decay amplitude  $D(B)^+ \rightarrow \sigma\pi^+$ :  
direct (6a) and polar (resonance) contributions (6b).

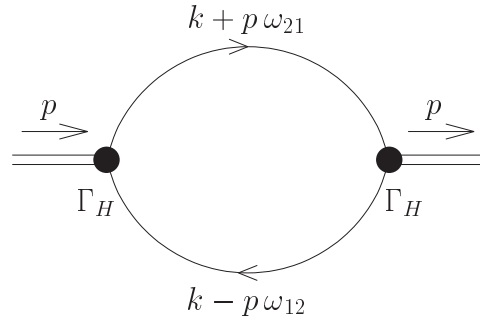
Fig.7: Electromagnetic form factor  $F_\pi(Q^2)$  of the pion in comparison to data taken from [46] (JLAB), [49] (DESY), [50] (CERN) and to other theoretical calculations: QCD sum rules [51], light-cone quark model [52], NJL model with a separable  $q\bar{q}$  interaction [53] and QCD modeling approach based on the solution of the Dyson-Schwinger equations [54].

Fig.8: Results for the pseudoscalar anomaly form factor  $Q^2 F_{\pi\gamma\gamma^*}(Q^2)$  in comparison to experimental data taken from [56] (CELLO), [40] (CLEO) and to other theoretical calculations: hard scattering approach (HSA) [57], QCD sum rules [58] and perturbative light-cone QCD [59].

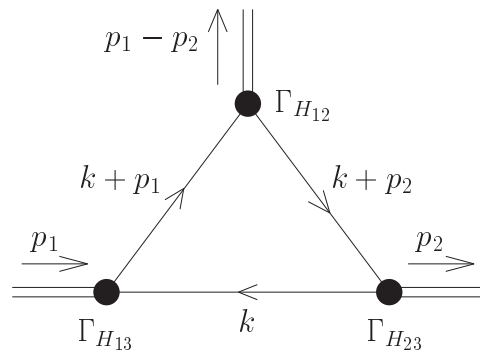
Fig.9: Our result for the form factor  $Q^2 F_{\pi\gamma^*\gamma^*}(Q^2, \omega)$  for different values of the asymmetry parameter  $\omega$ .

Fig.10: Our result for the scalar anomaly form factor  $Q^2 F_{\pi\gamma\gamma^*}(Q^2)$ . We also indicate the separate contribution of the dominant triangle ( $\Delta$ ) diagram.

Fig.11: Our result for the form factor  $Q^2 F_{\sigma\gamma^*\gamma^*}(Q^2, \omega)$  for different values of the asymmetry parameter  $\omega$ .



**Fig.1**



**Fig.2**

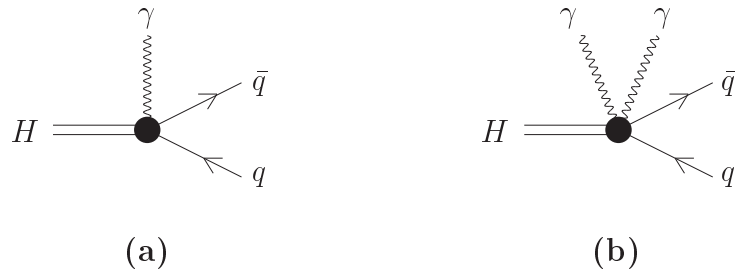


**Fig.3**

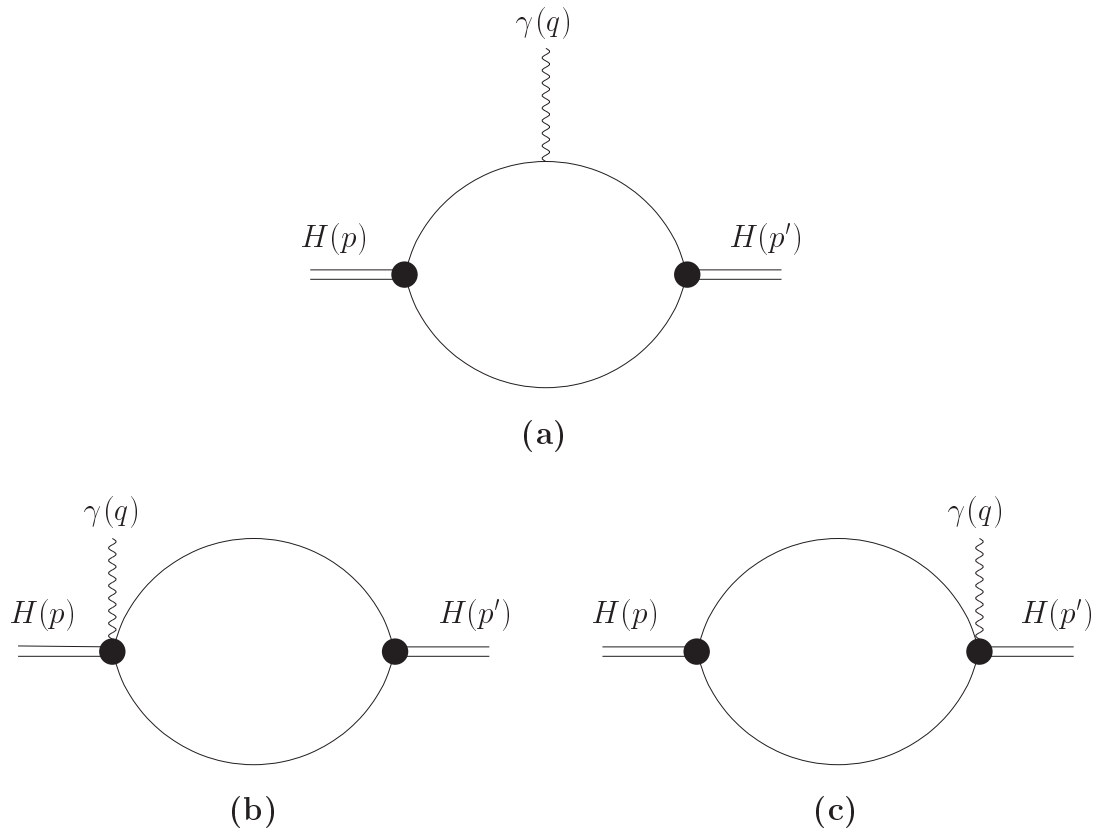


**Fig.4**

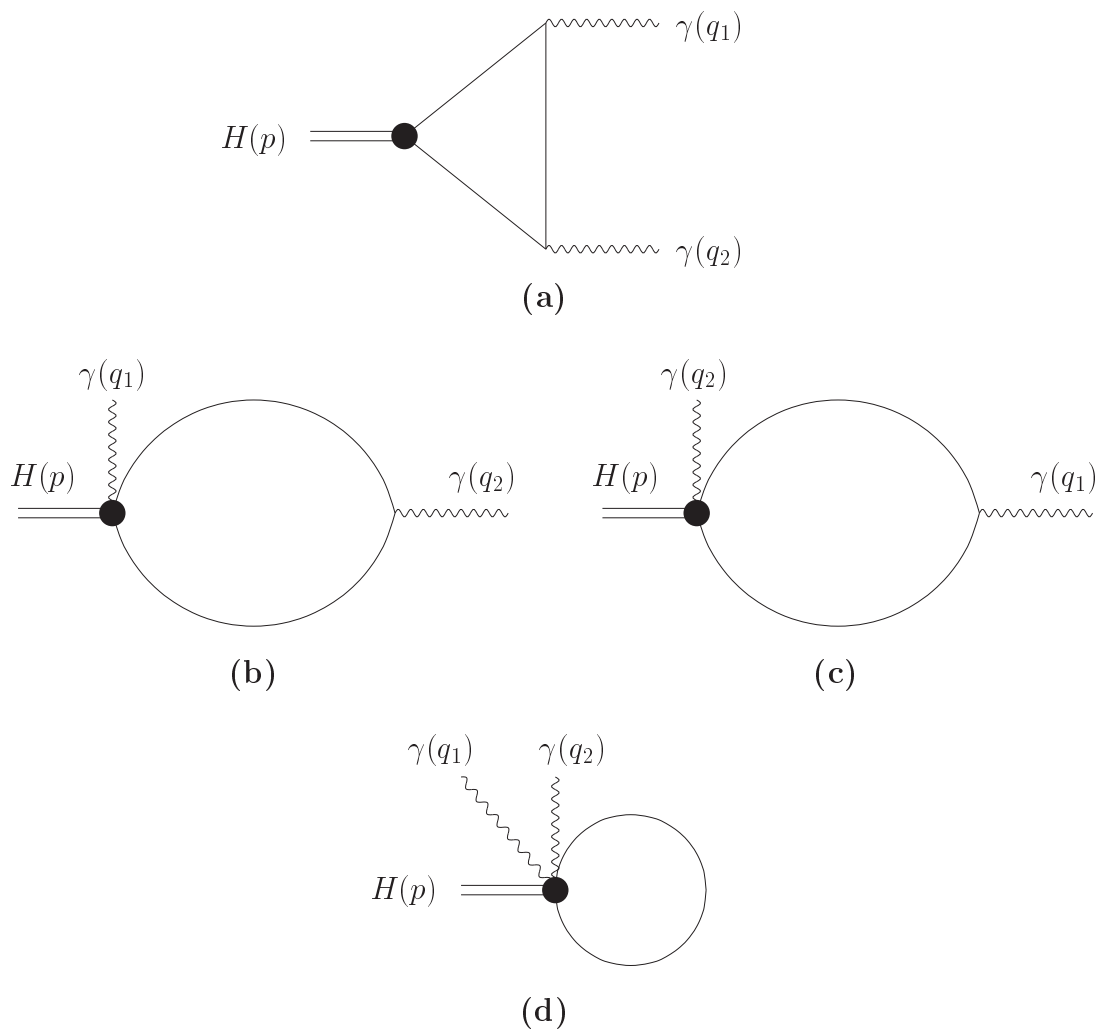
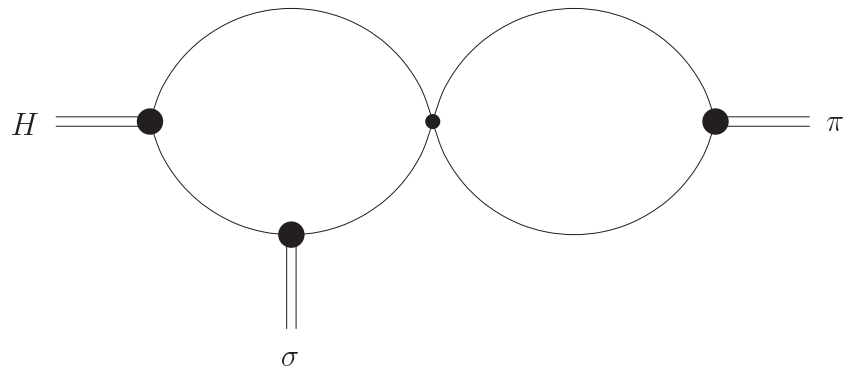
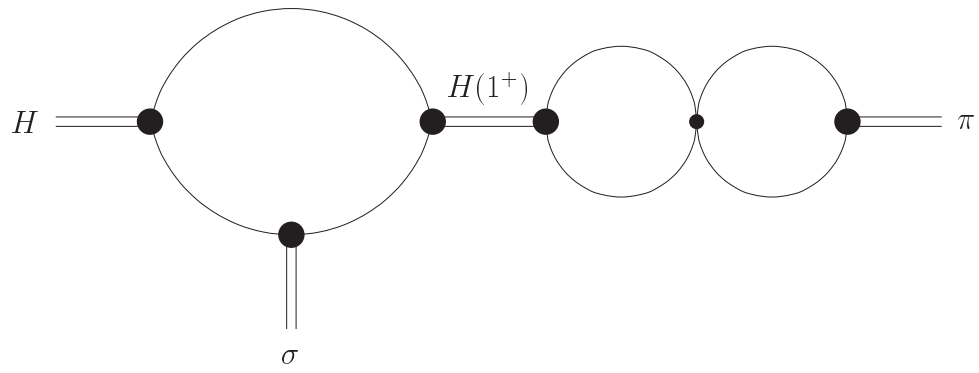


**Fig.5**



(a)



(b)

Fig.6

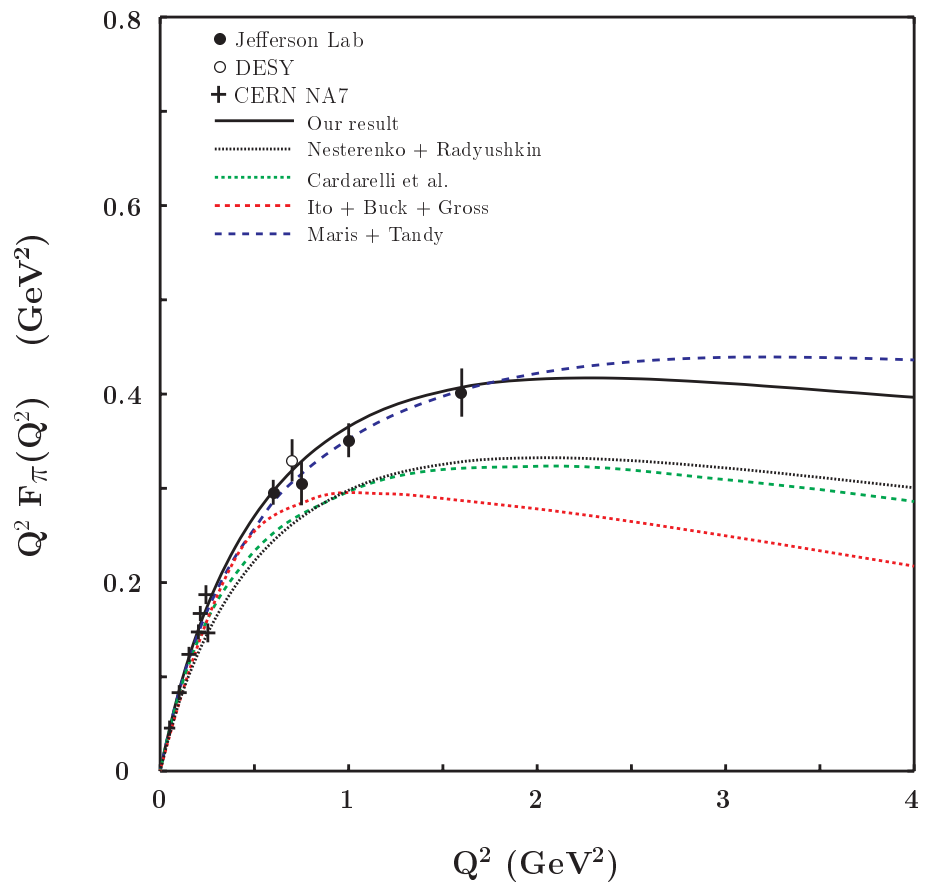


Fig.7

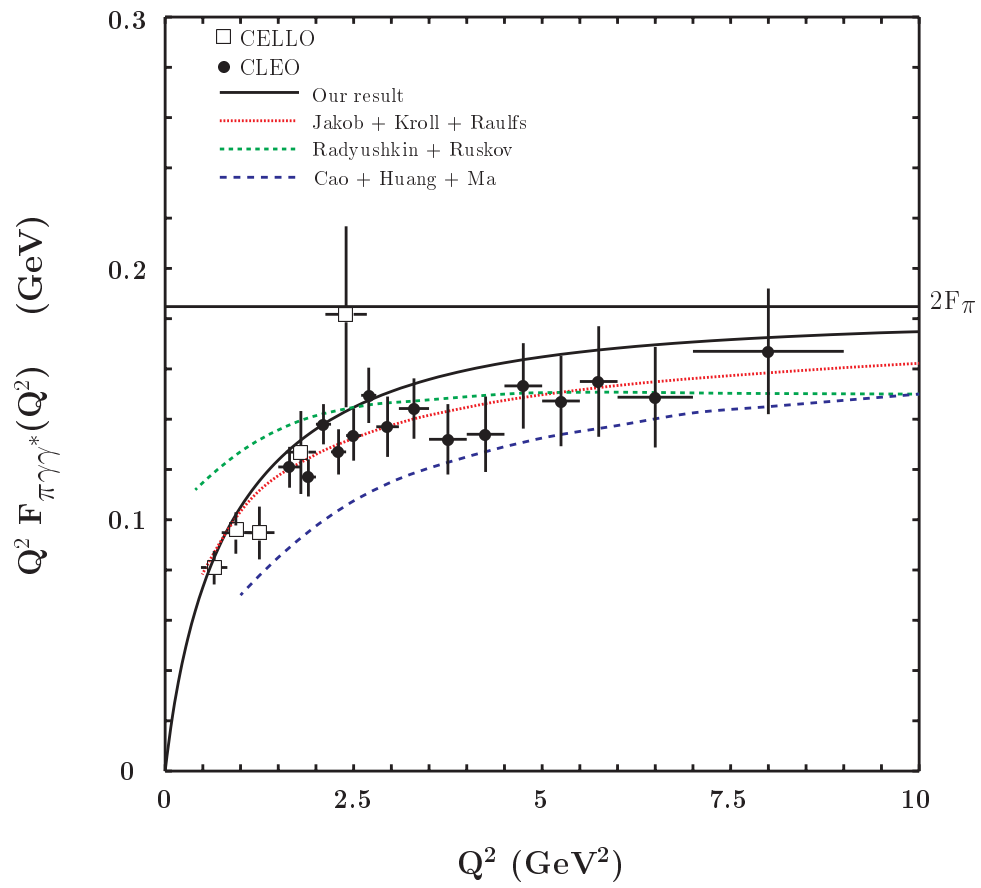


Fig.8

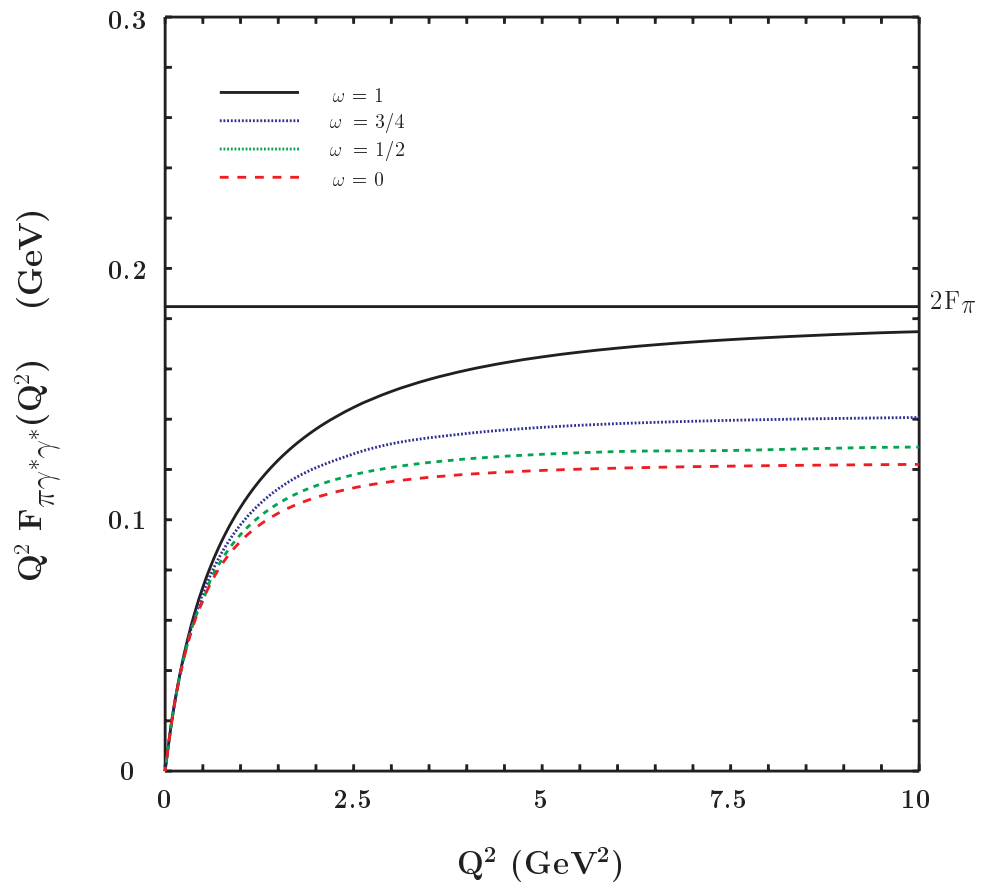


Fig.9

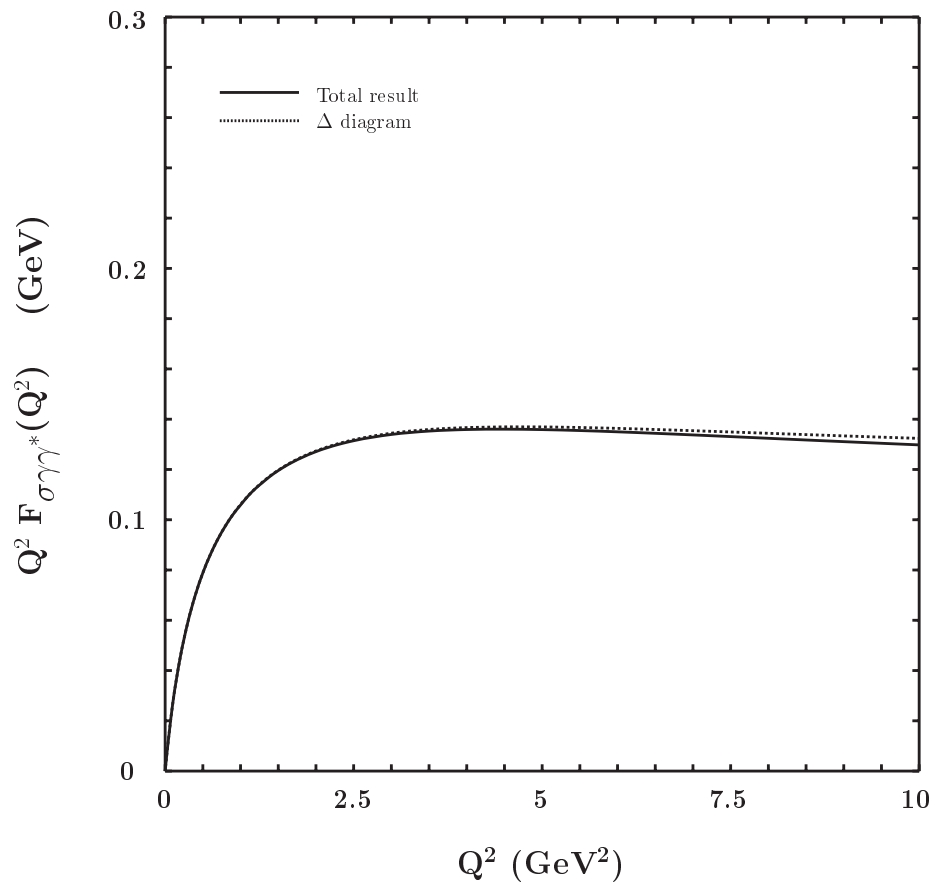


Fig.10

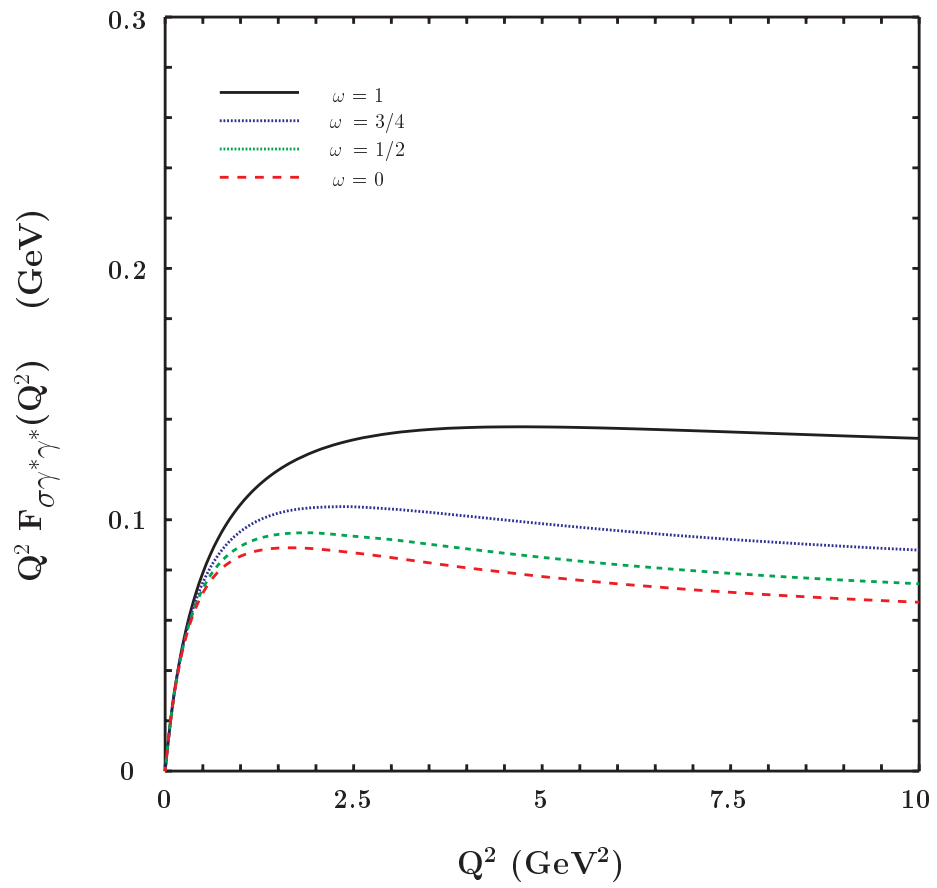


Fig.11